High-throughput phenotyping-based QTL mapping reveals the genetic architecture of the salt stress tolerance of *Brassica napus*

Guofang Zhang[1], Jinzhi Zhou[1], Yan Peng[1,2], Zengdong Tan[1], Yuting Zhang[1], Hu Zhao[1], Dongxu Liu[1], Xiao Liu[1], Long Li[1], Liangqian Yu[1], Cheng Jin[1], Shuai Fang[1], Jiawei Shi[1], Zedong Geng[1], Shanjing Yang[1], Guoxing Chen[1], Kede Liu[1], Qingyong Yang[1], Hui Feng[1,2]*, Liang Guo[1]* and Wanneng Yang[1,2]*

[1]*National Key Laboratory of Crop Genetic Improvement, Shenzhen Institute of Nutrition and Health, Huazhong Agricultural University, Wuhan, China*

[2]*Shenzhen Branch, Guangdong Laboratory for Lingnan Modern Agriculture, Genome Analysis Laboratory of the Ministry of Agriculture, Agricultural Genomics Institute at Shenzhen, Chinese Academy of Agricultural Sciences, Shenzhen, China*

*Correspondence: Wanneng Yang (ywn@mail.hzau.edu.cn), Liang Guo (guoliang@mail.hzau.edu.cn) and Hui Feng (fenghui@mail.hzau.edu.cn)

ABSTRACT

Salt stress is a major limiting factor that severely affects the survival and growth of crops. It is important to understand the salt tolerance ability of *Brassica napus* and explore the underlying related genetic resources. We used a high-throughput phenotyping platform to quantify 2,111 image-based traits (i-traits) of a natural population under 3 different salt stress conditions and an intervarietal substitution line (ISL) population under 9 different stress conditions to monitor and evaluate the salt stress tolerance of *B. napus* over time. We finally identified 928 high-quality i-traits associated with the salt stress tolerance of *B. napus.* Moreover, we mapped the salt stress-related loci in the natural population via a genome-wide association study (GWAS) and performed a linkage analysis associated with the ISL population, respectively. The results revealed 234 candidate genes associated with salt stress response, and two novel candidate genes, *BnCKX5* and *BnERF3*, were experimentally verified to regulate the salt stress tolerance of *B. napus*. This study demonstrates the feasibility of using high-throughput phenotyping-based QTL mapping to accurately

and comprehensively quantify i-traits associated with *B. napus*. The mapped loci could be used for genomics-assisted breeding to genetically improve the salt stress tolerance of *B. napus*.

Key-words: Brassica napus, high-throughput phenotyping, salt stress, GWAS, linkage analysis

INTRODUCTION

Crops are severely affected by salinity in many areas worldwide (Morton et al., 2019; Song and Liu, 2017). Saline land alone has been estimated to incur agricultural losses equal to approximately $30 billion (Qadir and Oster, 2004; Tyerman and Munns, 2019). Although breeders have used many approaches to produce high-yielding crops that can be harvested to meet the food needs of the growing population, maintaining global food supplies is a challenge (Hickey et al., 2019; Yamaguchi and Blumwald, 2005; Zhu, 2001).

The salt stress response is a complex genetic mechanism that is driven by the activation of a series of complex gene networks involving signal transduction, hormone regulation, epigenetic modification, transcriptional regulation, ion transporters, metabolic pathways, etc. (Wani et al., 2013). Salt stress conditions result mainly in osmotic and ionic stresses. The osmotic stress response is regulated usually by the abscisic acid (ABA)-dependent pathway, and this stress increases the water loss of plants under salt stress conditions (Kumar et al., 2013; Munns and Tester, 2008). Ionic stress arises when plant cells absorb and accumulate a large amount of Na^+ and Cl^- for a long period, which causes ion toxicity, especially in older leaves (Tester and Davenport, 2003). Salt stress-related signal transduction pathways include mainly ABA-dependent pathways, ABA-independent pathways, Ca^{2+} ion pathways, the salt overly sensitive (*SOS*) pathway and reactive oxygen species (*ROS*) pathways (Kumar et al., 2013). Multiple transporters and ion channels such as the Na^+/H^+ antiporter *SOS1* (Shi et al., 2002), the Na^+/H^+ exchanger *NHX* (Berkowitz and Masmoudi, 2007), the high-affinity potassium transporter *HKT1*, the vacuolar

pyrophosphatase *AVP1*, and the H^+ pyrophosphatase *TVP1* as well as nonselective cation channels have been shown to play important roles in maintaining cell- and plant-level ion homeostasis during salt stress (Gaxiola et al., 2001; Julkowska and Testerink, 2015).

Brassica napus is a vital oil crop species worldwide. Application of exogenous glycine betaine and proline at the germination and seedling stages can improve *B. napus* (Athar et al., 2009), and *AtNHX1* overexpression in *B. napus* can increase salt tolerance (Zhang et al., 2001). Seventy-five single-nucleotide polymorphisms (SNPs) have been revealed to be associated with *B. napus* (Wan et al., 2017). A total of 12 quantitative trait loci (QTLs) explaining 4.9% to 10.9% of phenotypic variation during salt stress have been mapped to different chromosomes (Jian et al., 2014). Approximately 45 QTLs for 10 salt stress tolerance indicators were identified in *B. napus* via an $F_{2:3}$ population (Lang et al., 2017). These studies of *B. napus* have focused mainly on the evaluation of salt stress tolerance, gene expression analysis and QTL mapping. However, the complex genetic basis and molecular mechanism underlying the *B. napus* salt stress response are largely unknown.

Salt stress tolerance involves various molecular, physiological and metabolic processes controlled by a large number of loci (Al-Tamimi et al., 2016; Guo et al., 2018). Genetic analysis enables the detection of loci or genes related to the salt stress response through the use of traditional agricultural or physiological indexes measured by conventional methods, which are low throughput, have a high degree of error, are nonstandard, are expensive and are labor intensive. In recent years, the use of high-throughput phenotyping platforms has gradually become an effective way to obtain high-quality standardized data (Li et al., 2020a; Yang et al., 2014), and many associated loci have been identified in *Arabidopsis*, rice, wheat, maize, *B. napus*, etc. RGB and chlorophyll fluorescence imaging have been used to estimate the growth and photosynthesis-related traits of *Arabidopsis* under salt stress (Awlia et al., 2016; Wu et al., 2021). Similarly, hyperspectral (GGP) imaging has been used as a high-throughput tool to measure various traits of maize plants, including agricultural,

chemical and physiological indicators (Ge et al., 2019; Ge et al., 2016). Loci associated with the salinity tolerance of rice have been identified by the combination of high-throughput phenotyping and genome-wide association studies (GWASs) to determine relative growth rates, transpiration rates, and transpiration use efficiency (Al-Tamimi *et al.*, 2016). Genetic loci associated with traits of *B. napus* roots have been identified by high-throughput root phenotyping (Shi et al., 2013). High-throughput phenotyping has also been used to parse the dynamic genetic architecture driving plant growth and yield (Li et al., 2020b; Wu *et al.*, 2021). In summary, the application of high-throughput phenotyping greatly accelerates the dissection of the complex genetic architecture of crop plants.

To study *B. napus* under salt stress response, image-based traits (i-traits), including 54 side-view (CS)-derived and 17 top-view (DS)-derived RGB-derived traits and 2,040 hyperspectrum-derived traits, were estimated via a high-throughput phenotyping platform from a natural population and an intervarietal substitution line (ISL) population. QTLs associated with salt stress tolerance were identified and compared by an i-trait-based GWAS and linkage analysis. We predicted 234 candidate genes associated with the salt stress response, and two unreported genes, *BnCKX5* and *BnERF3* located on ChrA02 and ChrA06, respectively, were experimentally verified to regulate the salt stress tolerance of *B. napus*. Additionally, some salt-tolerant and salt-sensitive accessions have been identified as breeding materials for genetic improvement of salt stress tolerance of *B. napus*. It proved to be trustworthy that the original images and genotypic and phenotypic data-based GWAS and linkage analysis of all 505 *B. napus* accessions and 91 ISLs are evaluated salt stress response in *B. napus*. Our study provides a promising method to reveal the genetic architecture involved in the genetic improvement of *B. napus*.

MATERIALS AND METHODS

Materials

A natural population consisting of 505 *B. napus* accessions was used in this study

(Supporting Information Table S1) (Tang et al., 2021). We also used a rapeseed ISL population comprising 91 lines as experimental materials (Supporting Information Table S1) (Li *et al.*, 2020b).

Stress treatments and high-throughput phenotyping

Five to six seeds (3 replicates per line) were directly sown in pots filled with 4.5 kg of soil on October 4, 2016 (for the 505 *B. napus* accessions), and October 4, 2018 (for the 91 ISLs), all of which were sown in one day. After sowing, all the plants were watered normally, and organic matter was applied. Fertilization with 200 mL of liquid fertilizer was carried out monthly (60 kg of water + 370.68 g of carbamide + 330.76 g of potassium dihydrogen phosphate + 94.24 g of potassium chloride; fully dissolved) (Guo *et al.*, 2018).

When they reached the 4–5 leaf-stage, the 505 *B. napus* accessions were cultivated outdoors in pots under control and low salt (L, 0.2%) and high salt (H, 0.4%) conditions and assessed via high-throughput phenotyping (Supporting Information Table S2). Due to the outdoor rainwash, we applied 0.05% salt or other treatments at two different time periods. We used RGB and GGP imaging at the first three time points (T1–T3), but we used only RGB imaging at the last two time points (T4–T5). In addition, we cultivated 91 ISLs in pots to which many various stress conditions were imposed, including low salt (LY, 0.2%), high salt (HY, 0.4%), low alkali (LJ, 0.15%), high alkali (HJ, 0.25%), low salt and low alkali (LYLJ, LY: 0.2% and LJ: 0.15%), low salt and high alkali (LYHJ, LY: 0.2% & HJ: 0.25%), high salt and low alkali (HYLJ, HY: 0.4% & LJ: 0.15%) and high salt and high alkali (HYHJ, HY: 0.4% and LJ: 0.25%) stress conditions (3 replicates per line), which were assessed via the high-throughput phenotyping platform. For the 91 ISLs, we used only the RGB images of plants under the various salt and alkali stress conditions during the T1–T5 periods. The entire experimental design, measurement time points, trait descriptions, weather conditions, and stress imposition methods are described in detail in Supporting Information Table S17.

High-throughput phenotyping image analysis and trait extraction

146 The processing of CS-derived RGB images involved the following 5 steps: 1) A
147 predefined rectangular block was used to remove the conveyor and other impurities
148 from the original CS images and obtain cropped images; 2) Hue, saturation, and
149 intensity (HSI) segmentation was used to obtain segmented binary images from the
150 previous RGB image and to calculate the morphology-related traits; 3) Other
151 morphology-related traits were calculated using the image convex hulls, which were
152 obtained through the binary image processing in step 2. 4) The binary images were
153 used as masks of the image obtained in step 1 to process the RGB images and the
154 corresponding gray images of the intensity channel, after which the color-related traits
155 and histogram texture-related traits were calculated from these images; and 5) Twenty
156 CS images were ultimately generated, and the i-traits of each sample were obtained
157 (Supporting Information Table S4) (Li *et al.*, 2020b).

158 The processing of the DS images was similar to that of the CS images and
159 involved 3 steps that differed from those for the CS images processing: 1) A
160 predefined rectangular block was used to remove the conveyor and other impurities
161 from the original DS images and to obtain the cropped images; 2) Excessive green (E
162 x G) segmentation was used to obtain segmented binary images from the original
163 DS-derived RGB image and then calculate the morphology-related traits; and 3) The
164 binary images were used as masks of the original DS image, and the histogram texture
165 trait- and color-related traits were calculated for the processed RGB image, gray
166 image of the intensity channel, gray image of the green channel, etc. (Supporting
167 Information Table S5) (Li *et al.*, 2020b).

168 A GGP imaging system was used for the first time to measure 505 accessions
169 under different salt stress conditions. We also provided a flow chart describing the
170 GGP image processing that included 3 main steps: 1) A binary data stream was
171 obtained for one sample from the HSI imaging system, and these binary data streams
172 were reorganized ultimately to obtain 250 GGP images (Supporting Information
173 Table S3). 2) Two of these 250 GGP images were selected for segmentation to obtain
174 new gray binary images, which were then processed; and 3) The binary images in step

2 were used to mask the 250 GGP images, which were subsequently processed to calculate the spectral traits, including the total reflectance-related traits, average reflectance-related traits, and logarithm-related traits (Supporting Information Table S6) (Wu *et al.*, 2021).

Image processing (CS, DS and GGP image analyses) was performed using LabVIEW 2015 (National Instruments, USA), which involved the use of a dynamic link library with Visual Studio 2015 (Microsoft, USA) and Open CV 3.4 (Open Source: https://github.com/fenghuifh2006/Maize-RGB-CT-HSI-program/tree/main/Maize-HSI-Program, https://github.com/fenghuifh2006/2-top_features_Rape-phenotyping and https://github.com/fenghuifh2006/3-side_features_Rape-phenotyping).

Destructive measurements for evaluating the high-throughput phenotyping platform

Twenty random accessions were grown and measured to evaluate the measurement and performance of the high-throughput phenotyping platform, and a reliable and robust model was constructed to assess and predict traditional agricultural traits of the plants under 3 salt stress conditions at 5 time points through destructive sampling and through nondestructive measurements by the high-throughput phenotyping platform, which included CS RGB-derived measurements, DS RGB-derived measurements, GGP measurements and manually measurements of traditional agricultural and physiological traits (Supporting Information Table S7).

Leaf chlorophyll content

Leaf chlorophyll content was measured under salt stress and control conditions using a SPAD-502 Plus chlorophyll meter (Spectrum Technologies, Inc.). Fully expanded penultimate leaves were used for the measurements. Each leaf was measured three times at different positions while avoiding the veins, and the average of the three readings was recorded for the different time points and under different stress conditions (Kang et al., 2019).

Determination of proline levels

Proline is an important component of the salt stress response of plants. The proline concentration was determined using a standard curve of L-proline. Approximately 0.1 g of leaf tissue was homogenized in 1.5 ml of 3% sulfosalicylic acid, and the residue was removed by centrifugation at 3000 rpm for 5 min each. One hundred microliters of the extract, 2 ml of glacial acetic acid and 2 ml acid ninhydrin (1.25 g of acid ninhydrin warmed in a solution comprising 30 ml of glacial acetic acid and 20 ml of 6 M phosphoric acid until it dissolved) were allowed to react for 60 min at 100 °C, and the reaction was then terminated by placement in an ice bath. The reaction mixture was extracted with 1 ml of toluene, after which it was vortexed for 30 seconds and incubated at room temperature for 10 min. Afterward, chromophore-containing toluene was warmed to room temperature, and its optical density at 520 nm was measured (Bates et al., 1973; Khedr and A., 2003).

Determination of malondialdehyde (MDA) content

We weighed and obtained approximately 0.1 g of leaf tissue, to which we added 2 ml of 10% trichloroacetic acid (TCA) solution followed by additional TCA such that the total volume was 3 ml and subsequently centrifuged the sample for 10 min at 4000 rpm. We transferred 2 ml of the supernatant into new tubes and added 2 ml of distilled water and 2 ml of 0.6% thiobarbituric acid (TBA) solution to another sample in boiling water for a 15 min reaction, after which the solution was centrifuged and cooled. Finally, we measured the MDA content at wavelengths of 450 nm, 532 nm and 600 nm via an ultra-microporous plate (MPP) spectrophotometer (BioTek Epoch, USA) (Shao et al., 2005; Wang et al., 2006).

Relative electrical conductivity (REC)

REC measurements were performed as previously described with minor modifications. One fully expanded functional leaf from normal plants was cut into segments of similar sizes and immersed in 8 ml of double distilled water in a 10 ml tube for 24 h at room temperature with continual shaking at 100 rpm, and then we calculated the REC by a conductivity meter. Then, this tube was boiled with water for 15 min of reaction cooling, and the REC was calculated by a conductivity meter (Model DDS-IIA,

Shanghai Leici Instrument, Inc., Shanghai, China).

Determination of the high repeatability, high heritability and significant treatment effect of traits related to the salt stress response

To select traits that had high repeatability, high heritability and significant treatment effects and that were related to the salt stress response, we developed a series of processes, as outlined here. 1) For outlier detection, using R language, we used the probability of data appearing outside the range of "±3σ" as P (| x-μ | >3σ) <= 0.3%. 2) Repeatability was measured according to the strength of the correlation coefficient (R_MAX) among 3 replicates, calculated via R language (Chen et al., 2014b). 3) For the heritability test, we calculated the H_2b of the traits as follows: $H_2b = \sigma^2_G /(\sigma^2_G + \sigma^2_{GE} /n + \sigma^2_e /nr)$. This was subjected to analysis of variance (ANOVA) using the lme4 package in the R environment (Chen *et al.*, 2014a; Li *et al.*, 2020b). 4) The genetic effect (G_effect), treatment effect (E_effect) and interaction effect of the genetic and treatment effects (G x E effect) represented the fixed effects of the genotype, the environmental effect of the experiment and the genotype-by-experiment interaction effect, respectively. Unlike for the controls, we calculated all the genetic and treatment effects of all traits using the AVOVA function in the R environment (Chen et al., 2014b). 5) For selected traits significantly associated with the salt stress response, by combining outlier screening, the repeatability of 3 replicates (R_MAX ≥ 0.5), dynamic heritability analysis (H2b ≥ 0.5) and the treatment effects (P_value ≤ 0.05) at different time points meeting these criteria, we ultimately obtained effective traits by the use of a strict screening system (Supporting Information Table S9) (Chen et al., 2014b).

Correlation network of i-traits and traditional agricultural traits

To link the high-throughput phenotyping-measured traits and traditional agricultural and physiological traits that were destructively measured, we performed correlation analyses of the i-traits and the traditional traits to construct a large correlation network encompassing different growth periods and stress conditions (Pearson's correlation coefficient (R) ≥ 0.3, P<0.001). The correlation network was visualized using Gephi

0.9.2 (NetBeans, open source).

Nondestructive prediction model and 5-fold cross validation

The use of high-throughput phenotyping platforms is gradually becoming an effective way to collect high-quality standardized data over time. To improve the data collection efficiency and standardization, reduce manual error and reduce labor costs, we used stepwise regression analysis to develop a series of nondestructive prediction models via destructive measurements, which was implemented with SPSS Statistics 25 (IBM, USA) (Supporting Information Table S10).

To understand the generalizability of the prediction model, we used 5-fold cross validation. The dataset was divided into five parts. A subset was taken as the validation set each time, and the remaining data were taken to compose the training set to obtain the index of the fitting effect of the current training model expressed by the Mean absolute error (MAE). After this process was repeated five times, many MAEs of each model were compared, and parameters corresponding to the minimum MAE value were used as the optimal models and parameters. Fivefold cross validation was implemented with LabVIEW 2015 (National Instruments, USA) (Supporting Information Table S10).

GWAS

A total of 505 *B. napus* accessions were used to construct an association panel. Their high-quality clean read data were analyzed by BWA (v0.75) software (Li and Durbin, 2009). The reference genome information was obtained from the *Brassica* v4.1 ('Darmor-bzh') genome (http://www.Genoscope.cns.fr/brassicanapus/data/). We adopted a mixed-model approach using a factorial spectrally transformed linear mixed model that included 7,862,482 SNPs across the entire *B. napus* genome. We also performed GWASs using the FaST-LMM and GAMMA software models (Listgarten et al., 2013; Zhou and Stephens, 2012). The suggested and significant P-value threshold of the entire population was 1.0E−06. The candidate genes with different gene expression ratios between the control treatment and stress treatment ($R \geq 2$ or ≤ 0.5) and summary score (≥ 0.9) were within 200 kb upstream or downstream of the

lead SNP (Supporting Information Table S11-12) (Tang *et al.*, 2021).

Linkage analysis

The 91 ISLs are described in detail in a previous study (Li *et al.*, 2020b; Zhang et al., 2015) and were sequenced using the genotype-by-sequencing (GBS) method in conjunction with 4,214 genotype markers throughout the whole genome. These markers covered approximately 350 substituted chromosome segments across the 19 chromosomes. A total of 2,223 tolerance coefficients (TCs) traits were determined using Ici-Mapping 4.1 software with the RSTEP-LRT-ADD model according to a LOD threshold of 2.5 (Meng *et al.*, 2015). The QTL intervals (between at least 2 marker intervals) were then defined as overlap hotspots according to the latest published ZS11 genome sequence (Song et al., 2020; Wu et al., 2019). Some genes or QTLs were selected as candidates within the 5M region upstream or downstream of a significant genotype marker (Supporting Information Table S11; Supporting Information Table S13) (Li *et al.*, 2020b; Zhang *et al.*, 2015).

LD analysis

LD analysis was performed with PLINK (Tang *et al.*, 2021).

RNA-seq

Total RNA was extracted with TRIzol reagent (Invitrogen Life Technologies) from the leaves of 4-week-old plants grown in soil in a growth chamber set at a constant 25 °C temperature, a 16/8 h light/dark photoperiod and 50–60% relative humidity (RH). The RNA was dissolved in diethyl phosphorocyanidate (DEPC) water and measured with a spectrophotometer (NanoDrop 2000; Thermo Scientific, Waltham, MA). The purified RNA was sequenced with GenoSeq (high-throughput phenotyping://www.genoseq.cn/) using an Illumina HiSeq platform in paired-end 2x 150 bp mode, and approximately 10 Gb of clean reads were generated for each sample. We then filtered the low-quality sequences with Trimmomatic and calculated the normalized transcripts per million (TPM) values (Supporting Information Table S15).

Functional study of candidate genes

To verify functions of candidate genes under salt stress, the coding DNA sequences (CDSs) of BnaA02g05340D (*BnCKX5*) and BnaA06g02670D (*BnERF3*) were cloned from accession X182, and the cloned fragments were subsequently ligated into pCAMBIA-1300s using the KpnI and XbaI restriction enzymes (Supporting Information Table S16). Westar was used as the transgenic receptor material.

From July to September 2019 and from September to November 2020, we planted *OE-BnCKX5*, *OE-BnERF3* and Westar (WT) plants in a growth chamber set at a constant 25/16 ℃ day/night temperature, a 16/8 h light/dark photoperiod and 50–60% RH to measure PH and ADW. Each genotype was divided into two treatments: a control treatment and a salt stress treatment imposed via application of a 385 mM NaCl solution of liquid fertilizer (per large box: 30 L of water + 500 g of NaCl; ~385 mM). Each line included at least 6 biological replicates.

From early July to September 2020 and from late July to September 2020, approximately one-week-old uniform seedlings were transferred to Hoagland solution (4.0 mM KNO_3, 1.0 mM $MgSO_4$, 4.0 mM $Ca(NO_3)_2$, 1.0 mM $NH_4H_2PO_4$, 1.0 mM $(NH_4)_2HPO_4$, 1 mM NaCl, 41.2 μM Na_2-EDTA, 12.5 μM H_3BO_3, 0.39 μM $CuSO_4$, 1.59 μM $MnSO_4$, 1.0 μM $ZnCl_2$, and 0.5 μM $NaMoO_4$), the pH of which was adjusted to 5.8 with 0.1 M KOH. The growth conditions of the greenhouse included a 25/16 °C day/night temperature, a 16/8 h of light/dark photoperiod and 50–60% RH. Three-week-old plants were subjected to salt stress (0 mM, mM 50, mM 100 and 150 mM NaCl) for two weeks, and there were at least 8 biological replicates per treatment. Afterward, we measured the PH, ADW and REC traits.

From late September 2019 to early May 2020 (with only one environmental replicate and no high-throughput phenotyping) and from late September 2020 to early May 2021 (with two different environmental replicates and high-throughput phenotyping), first, 5–6 seeds were directly sown into pots filled with 4.5 kg of soil. After sowing, all the plants were watered normally, and organic matter was applied. Fertilization with 200 ml of liquid fertilizer was carried out per month (60 kg of water + 370.68 g of carbamide + 330.76 g of potassium dihydrogen phosphate + 94.24 g of

potassium chloride; fully dissolved). Each genotype, including at least 3 independent transgenic lines with at least 8 biological replicates per line, was divided into two treatments for high-throughput phenotyping—a control treatment and salt stress treatment via fertilization with approximately 500 ml of a 385 mM NaCl solution of liquid fertilizer per pot (30 L of water + 500 g of NaCl; ~285 mM NaCl).

Data availability

The CS RGB-derived, DS RGB-derived, GGP and traditional traits are shown in Supporting Information Table S3-S7. The significant candidate SNPs, QTLs and genes associated with the salt stress response are listed in Supporting Information Table S11-S13. All of the original high-throughput phenotyping images, phenotypic data, genotypic data and image analysis processes for the different stress conditions have been added to the Huazhong Agricultural University high-throughput phenotyping platform database. We are also very happy to provide reasonable help involving our original images and data, research materials and methods if the corresponding authors are contacted.

RESULTS

High-throughput phenotyping of *B. napus* under stress conditions

To explore the genetic basis of the salt stress tolerance of *B. napus*, we used two populations: a population of 505 *B. napus* accessions (Tang et al., 2021) and a population 91 ISLs (Supporting Information Table S1) (Li *et al.*, 2020b). The 505 *B. napus* accessions were cultivated in triplicate under normal (CK), low (L, 0.2% NaCl) and high salt stress (H, 0.4% NaCl) conditions at the Huazhong Agricultural University and evaluated via a high-throughput phenotyping platform (Fig. 1a; Supporting Information Table S2). At the same time, 20 accessions (3 replicates) at 5 time points were automatically and manually measured to evaluate the correlation between the i-traits and manually measured traits. In addition, we cultivated 91 ISLs under 9 stress conditions, with 3 replicates per line (Supporting Information Table S2). For the 505 accessions, the dynamic salt stress response of each plant was captured by

RGB imaging at 5 time points (CS1-CS5 for the CS and DS1-DS5 for the DS) and GGP imaging at 3 time points (GGP1-GGP3 for the GGP view) (Fig. 1b). In total, we collected 8.3 terabytes of images, which consisted of 454,500 CS-derived RGB images (3.9 terabytes), 22,725 DS-derived RGB images (0.2 terabytes) and 13,635 GGP images (4.2 terabytes). For the 91 ISLs, each plant was evaluated via RGB imaging at 5 time points (CS1-CS5 for the CS and DS1-DS5 for DS). In total, we collected 2.3 terabytes of imagery, which included 245,700 CS-derived RGB images (2.1 terabytes) and 12,285 DS-derived RGB images (0.1 terabytes). Finally, we measured several traditional traits manually. In summary, these indicators could be classified into five categories throughout the whole growth period: geometric or morphological indexes, physiological indexes, GGP indexes, traditional agricultural traits and quality indexes (Supporting Information Table S3).

After the original images were obtained, we used an automatic image analysis pipeline (Li *et al.*, 2020b) to extract the i-traits, which involved 54 CS images of RGB-derived i-traits (Supporting Information Table S4) and 17 DS images of RGB-derived i-traits of the 505 accessions and 91 ISLs (Fig. 1c; Supporting Information Table S5). A total of 2,040 GGP i-traits were extracted from the images of the 505 accessions (Fig. 1c; Supporting Information Table S6), and RGB-derived and hyperspectrum-derived i-traits and manually measured traits were assessed for 20 accessions (Supporting Information Table S7). We named these i-traits measured under different treatment conditions and stages according to the suffix type “trait name_time point_treatment”, e.g., E_TEX_SV_CS1_CK. To better evaluated the salt stress response, we focused on the salt tolerance coefficient (STC), calculated as the ratio of trait values under salt stress conditions and to those under normal conditions at different time points, which is represented by the suffix type “trait name_time point_treatment_D_control”, e.g., E_TEX_SV_CS2_LDCK. In total, 8,792 original i-traits, including 432 CS RGB-derived traits, 136 DS RGB-derived traits, 8,160 hyperspectrum-derived (GGP) i-traits and 64 traditionally derived (destructively obtained) traits, were assessed and further analyzed (Fig. 1c) (Guo *et al.*, 2018). To

process the large amount of data collected, we developed a strict data analysis pipeline to select i-traits related to the salt stress response (Fig. 1d).

Determining reliable i-traits related to the salt stress response with high repeatability, high heritability and significant treatment effects under salt stress

To quantify the data, we created a series of filter conditions by a threshold-based filtering procedure (median ± 3 SDs (standard deviations)) and assessed the repeatability among the 3 biological replicates. The filter standard for repeatability was a median correlation coefficient greater than 0.5 (R_MAX ≥ 0.5). In the end, we selected 27 (50% of the total), 28 (51.9% of the total), and 28 CS-derived traits (51.9% of the total) for the control, low salt stress and high salt stress conditions, respectively. We selected 12 (70.6% of the total), 11 (64.7% of the total) and 10 DS-derived traits (58.8% of the total) for the control, low salt stress and high salt stress conditions, respectively. For the hyperspectrum-derived (GGP) traits, including any derived characteristics (GGP_marker), we also selected 2,024 (99.2% of the total), 1,776 (87.1% of the total) and 2,030 GGP traits (99.5% of the total) for the control, low salt stress and high salt stress conditions, respectively. These i-traits showed high repeatability across all 3 replicates (after the outliers were removed) (Fig. 2a). The descriptive statistics, dynamic heatmap and the clustering diagram trends of the salt stress response of the i-traits indicated dynamic changes and variation under salt stress (Fig. 1a–d; Supporting Information Table S8).

Heritability is a key factor that is commonly applied in crop science (Holland et al., 2010). Here, we first calculated and analyzed the dynamic changes in broad-sense heritability (H_2b) for the 505 accessions and 91 ISLs under salt stress over time. Approximately 64% of i-trait H_2b values were greater than 0.5 (Fig. 2b); the genetic effect (G_effect) and treatment effect (E_effect) represent the genotypic effect and environmental effect, respectively (Chen et al., 2014b). We filtered these traits by low salt and high salt treatment effects compared with the control effect, (L_treatment effect and H_treatment effect, P_value ≤ 0.05), which were significant under low and high salt stress. To choose the effective i-traits associated with the salt stress response,

436 we combined a high heritability median (H2b ≥ 0.5) and a significant low salt
437 treatment effect and obtained 1,141 (54.05%) traits. At the same time, we obtained
438 1,287 (60.97%) traits with high heritability and high salt treatment effects. In terms of
439 the stability across the three replicates, we combined the median dynamic R_MAX
440 and low treatment effect, and we ultimately selected 1,801 (85.32%) traits. For the
441 dynamic median R_MAX and H_treatment effects, a total of 1,978 (93.6%) traits
442 were selected (Fig. 2c; Supporting Information Table S9). Finally, via strict filtering
443 criteria, we obtained 928 traits associated with the salt stress response (Fig. 2d;
444 Supporting Information Table S9) (Chen et al., 2014b).

445 **I-traits as salt stress biomarkers for predicting traditional traits**

446 To predict traditional agronomic traits including plant height (PH), aboveground fresh
447 weight (AFB), aboveground dry weight (ADB), leaf area (LA), stem dry weight
448 (Stem_DW), stem fresh weight (Stem_FW) and chlorophyll content (SPAD), we
449 developed a series of nondestructive methods involving model construction (Fig.
450 S2-S4). From the prediction results, most of the predicted indicators' adjusted
451 coefficients of determination (R^2) were greater than 0.8 according to stepwise
452 regression analysis and 5-fold cross-validation (Supporting Information Table S10).
453 Using the prediction model, we predicted the ADB, AFB and PH over time (Fig. S5).
454 Taken together, these results demonstrated that our i-trait-based prediction model
455 could be used to predict the agronomic traits of *B. napus* under salt stress in the
456 future.

457 **Dissection of the genetic basis of *B. napus***

458 The relative value of traits between control and treatment conditions is usually
459 described as the main salt stress indicator of the growth and development of plants
460 under salt stress (Guo *et al.*, 2018). For the natural population, we performed a
461 GWAS of 2,246 STCs, including those from 324 CS RGB-derived traits, 102 DS
462 RGB-derived traits, 1,756 hyperspectrum-derived (GGP) traits and 64 manually
463 measured traits, via a linear mixed model with Fast-LMM (Listgarten et al., 2013) and
464 GEMMA for GWAS (Supporting Information Table S11) (Zhou and Stephens, 2012).

For the 91 ISL populations, we used ICI-Mapping to map salt stress-related QTLs via linkage analysis involving 2,132 tolerance coefficients (TCs) of RGB-derived traits at different time points and under different salt stress conditions (Supporting Information Table S11) (Meng et al., 2015).

With respect to the GWAS analysis, we identified a total of 657,136 significant SNPs (Supporting Information Table S12). For the manually measured traits, we identified 5,531 significant SNPs associated with the salt stress response. However, we identified 283,227 SNPs significantly associated with GGP traits; this method was more effective than traditional methods to identify additional SNPs related to the salt stress response. A total of 1,197 significant SNPs (21.64% of 5,531 significant SNPs identified via manually measured traits) colocalized with the significant SNPs associated with the i-traits (Fig. 3a). We also assessed the effects of these significant SNPs associated with the salt stress response, which were significantly different from the effects of random SNPs (Fig. 3b). The numbers of traits with colocalized SNP frequencies revealed different hotspot areas and distribution regions across the chromosomes (Fig. 3c). To avoid possible false-positive significant SNPs, we defined reliable SNPs related to the salt stress response as those with more than 10 colocalized SNPs (in terms of frequency), which presented different numbers of SNPs across the chromosomes (Fig. 3d; Supporting Information Table S12). Next, we quantified the traits sharing colocalized SNPs between the manually measured traits and i-traits. Almost half of the manually measured traits revealed colocalization of high-frequency SNPs with more than 50 i-traits, such as proline concentration, ADB, relative electrical conductivity (REC) and yield (Fig. 3e; Supporting Information Table S12). We ultimately focused on 2,814 high-frequency and colocalized SNPs detected between the CS RGB-derived traits, DS RGB-derived traits, hyperspectrum-derived (GGP) traits and manually measured traits within 234 candidate genes related to the salt stress response according to the candidate gene selection criteria (Tang *et al.*, 2021). Moreover, many previously reported genes related to the salt stress response, such as *SnRK2*, *RD20*, *SOS3*, *ABI5* and *WRKY33*, differentially expressed between

wild-type WT plants and salt-stressed plants were identified within the mapped QTLs (Fig. S6; Supporting Information Table S12). Moreover, for linkage analysis involving 91 ISLs, we identified 204 significant and high-frequency colocalized QTLs distributed across different chromosomes (Supporting Information Table S13) (Li et al., 2020b). Taken together, these results indicate that high-throughput phenotyping-based QTL mapping is an efficient way to reveal the complex genetic architecture associated with the salt stress response of *B. napus.*

BnCKX5 overexpression increases the sensitivity to salt stress

For GWAS analysis, we detected 57 high-frequency and colocalized SNPs, including 4 SNP clusters on ChrA02 (cluster I was from 2062941 to 2518619 bp; cluster II, 2753745 to 3206647 bp; cluster III, 11141835 to 11142240 bp; and cluster IV, 23011682 to 23478650 bp) from 2062941 to 24168754. Many vital colocalized SNPs for different types of traits were detected on ChrA02 via our GWAS: ADB_HDCK and SPAD_LDCK (manually measured traits); GPA_SV_CS5_HDCK and HA_SV_CS5_HDCK (RGB traits); and dA234_GGP2_HDCK, M4_HDCK_GGP3 and M20_HDCK_GGP3 (GGP traits) (Fig. 3f; Fig. S7a). In addition, the peak QTLs between markers A02_M1 (logarithm of odds (LOD) = 20.27) and A02_M26 (LOD = 9.26) of R_SV_CS4_LYLJ and marker A02_M31 (LOD = 4.87) of HWR_TV_DS4_HY colocalized on ChrA02 (Fig. S7b). For ChrA02 cluster I, there were approximately 50 genes within 200 kb upstream and downstream of the lead SNP BnvaA0202316797 associated with ADB based on pairwise linkage disequilibrium (LD) correlations ($R^2 > 0.5$) (Fig. 4a–4b). BnaA02g05340 was highly induced in response to salt stress and ABA treatment (Fig. 4c)**,** and it contained SNP variations leading to amino acid changes (Fig. 4d; Supporting Information Table S14). BnaA02g05340 is named *BnCKX5* and belongs to *CKX* subfamily VII; this gene encodes cytokinin oxidase/dehydrogenase, which catalyzes the degradation of cytokinins to maintain cytokinin homeostasis (Ma et al., 2016). Whether *CKXs* play a role in plant salt stress tolerance remains unknown (Liu et al., 2018).

The haplotypes of *BnCKX5* were grouped into haplotypes A, B and C (Fig. 4e–4i). The ADB of haplotype C under control, low and high salt stress was significantly higher than that under haplotype A and haplotype B (Fig. 4e–4g). However, in terms of ADB, the ranges of haplotype A ratio between low salt stress and the control (ADB_LDCK) conditions were significantly different from those of haplotype B and haplotype C but did not differ between haplotype B and haplotype C (Fig. 4h). In addition, in terms of ABD, the range of the haplotype B ratio (ADB_HDCK) between the high salt stress and control conditions was lower than that of the haplotype A ratio (Fig. 4i). Taken together, these results indicate that approximately 30 haplotype C-type accessions could be salt stress-resistant germplasms that are valuable resources for breeders (Supporting Information Table S14).

BnCKX5-overexpressing (*OE-BnCKX5*) and WT plants were grown in soil and treated with 285 mmol NaCl (Fig. 4j; Fig. S8d). *BnCKX5* was significantly induced in response to salt stress in the WT, and the *OE-BnCKX5* lines presented significantly higher expression levels than the WT plants did (Fig. 4k; Supporting Information Table S15). The ADB and PH significantly decreased for the *OE-BnCKX5* lines compared to the WT plants under salt treatment (Fig. 4l–4m). In addition, the ADB and PH were lower for *T_OE-BnCKX5* than for the WT (T_WT) under hydroponic salt conditions (0 mmol, 50 mmol, 100 mmol and 150 mmol) (Fig. 4n–4p; Fig. S8a–8c), and the REC of *OE-BnCKX5* was significantly higher than that of the WT under 50 and 100 mmol NaCl treatment conditions (Fig. 4q). Moreover, we used a high-throughput phenotyping platform to measure the transgenic lines at two different time points (Fig. 4r). Compared with the T_WT' trait, type many high-throughput phenotypic traits, such as the height of minimum circumscribed box in CS (H_SV) (Fig. 4s), the green projected area in CS (GPA_SV) (Fig. 4t), and the total projected area in CS (TPA_SV) (Fig. 4u), were suppressed under salt stress; other traits that were clearly affected are shown in Fig. S9. Taken together, the above results indicate that *BnCKX5* overexpression increases the sensitivity to salt stress. However, its detailed molecular mechanism of salt stress remains to be further investigated.

BnERF3 overexpression increases the resistance to salt stress

We obtained 36 high-frequency colocalized SNPs grouped into 3 clusters on ChrA06 (cluster I was from 1695085 to 2163217 bp; cluster II, 3062521 to 6618806 bp; and cluster III from 18159306 to 21636994 bp) via different types of trait-based GWASs. A series of different types of traits, such as ADB_HDCK and REC_LDCK (manually measured traits), HWR_TV_DS2_HDCK, FN_SV_LDCK_CS5 (RGB traits) and dT 204_GGP3_LDCK and M35_LDCK_GGP2 (hyperspectrum-derived traits), revealed many vital colocalized SNPs on ChrA06 via our GWAS (Fig. 3g; Fig. S10a). In addition, the peak QTLs between markers A06_M2 (LOD = 26.57) of U_TEX_SV_CS4_LY and A06_M2 (LOD = 10.97) of MU3_TEX_TV_HYLJ were found by linkage analysis to be colocalized on ChrA06 (Fig. S10b). For ChrA06 cluster I, there were approximately 40 candidate genes within 200 kb upstream and downstream of the lead SNPs BnvaA0601558949 and BnvaA0601662590 associated with ADB based on pairwise LD correlations ($R^2 > 0.5$) (Fig. 5a–5b). BnaA06g02670D was highly induced in response to salt stress and ABA treatment (Fig. 5c), and it contained SNPs leading to amino acid changes (Fig. 5d; Supporting Information Table S14). BnaA06g02670D is named *BnERF3* and encodes an ERF/AP2 transcription factor; however, whether this protein plays a role in plant salt stress tolerance remains unknown (Zhang and Huang, 2010). Overexpression of ERF family genes has been recently performed in *Arabidopsis*, rice, *B. napus*, tomato, etc., and was shown that it could improve the tolerance to many abiotic stresses (Aharoni et al., 2004; Song et al., 2005; Gao et al., 2008; Karaba et al., 2007; Ai-Sheng et al., 2012; Fischer and Droge-Laser, 2004).

The haplotypes of *BnERF3* were grouped into haplotypes A, B, C and D (Fig. 5e–5i). The ADB values of the 505 accessions with haplotype B and haplotype C were significantly higher than those of haplotype A and haplotype D. Moreover, the ADB of haplotype D of was lowest among those of the 4 haploid types under control and low and high salt stress conditions (Fig. 5e–5g). However, the ratio ranges of ADB (ADB_LDCK and ADB_HDCK) between the low and high salt stress

580 treatments and the control under haplotype C were larger than those of the other
581 haplotypes (Fig. 5h–5i). Regardless of the real ADB value and the ratio between the
582 treatment and control conditions, the ranges of haplotype B and haplotype C were
583 lower than those of the others. Taken together, these results showed that haplotype C
584 and haplotype D, which included 25 varieties, may be sensitive varieties and that
585 haplotype B, which included 10 varieties, may be resistant to salt stress; these
586 materials may be rich germplasm resources for breeders (Supporting Information
587 Table S14).

588 *BnERF3*-overexpressing (*OE-BnERF3*) and WT plants were grown in soil and
589 treated with 285 mmol NaCl (Fig. 5j; Fig. S11d). *BnERF3* was significantly induced
590 in response to salt stress in the WT, and compared with the WT plants, the
591 *OE-BnERF3* lines under salt stress presented significantly higher expression levels
592 (Fig. 5k; Supporting Information Table S15). ADB and PH significantly decreased for
593 the *OE-BnERF3* lines compared to the WT plants under salt treatment (Fig. 5l–5m).
594 In addition, the ADB and PH significantly decreased for *OE-BnERF3* lines compared
595 to the WT plants under hydroponic salt conditions (0 mmol, 50 mmol, 100 mmol and
596 150 mmol) (Fig. 5n–5p; Fig. S11a–c). However, the REC significantly increased in
597 the *OE-BnERF3* lines compared to the WT plants under salt treatment (Fig. 5q).
598 Finally, we used a high-throughput phenotyping platform to measure the transgenic
599 lines and WT plants at two different time points (Fig. 5r). Many i-traits, such as the
600 H_SV (Fig. 5s), GPA_SV (Fig. 5t) and TPA_SV (Fig. 5u), significantly decreased for
601 the *OE-BnERF3* lines compared to the WT plants under salt stress at the first time
602 point; other i-traits that were clearly affected are shown in Fig. S12. *BnERF3*
603 overexpression increases the resistance to salt stress. However, the regulation
604 mechanism of *BnERF3* involved in response to salt stress needs further investigation.
605

606 **DISCUSSION**

607 High-throughput phenotyping platforms could constitute one of the main bridges from
608 phenotype to genotype and have shown great advantages in promoting crop breeding

609 and in functional genomics (Yang et al., 2020). Previously, only RGB-derived traits
610 based on GWASs or QTL mapping have been used to reveal the genetic basis of crop
611 growth dynamics (Campbell et al., 2015; Xiaqing et al., 2019). In this study, we first
612 used a high-throughput phenotyping platform including RGB-derived and especially
613 hyperspectrum-derived indicators to reveal the salt stress response based on a GWAS
614 and linkage analysis. By using the high-throughput phenotyping image pipeline, we
615 obtained 54 CS RGB-derived traits, 17 DS RGB-derived traits and 2,040
616 hyperspectrum-derived (GGP) traits over time to reveal and evaluate the genetic
617 architecture of the salt stress tolerance of *B. napus* (Fig. 1). We identified a total of
618 2,111 traits, which consisted of some low-quality traits with low repeatability,
619 heritability or no significant treatment effect. We ultimately selected 928 high-quality
620 indicators associated with the salt stress response and extreme varieties for genetic
621 improvement of *B. napus* with high repeatability, a high H_2b and significant treatment
622 effects according to strict selection criteria (Fig. 2).

623 Compared with the RGB-derived traits, most hyperspectrum-derived traits strongly
624 reflected the salt stress response of *B. napus*, as shown by heatmap and clustering
625 trend chart analyses (Fig. S1). The CS RGB-derived traits, such as M_TEX_SV,
626 U_TEX_SV and GPA_SV, were significantly associated with the ADB at different
627 time periods and under treatment conditions. By using GGP imaging, we found that a
628 series of different wavelength ranges, such as lgT1~lgT20 and lgT150~lgT250, were
629 associated with ADB. CS RGB-derived traits including SE_TEX_SV, S_TEX_SV and
630 GPA_SV were strongly correlated with PH. Chlorophyll fluorescence imaging can be
631 used to detect early and late changes in response to salt stress (Awlia *et al.*, 2016; Ge
632 *et al.*, 2016). Chlorophyll content is considered a key factor in stress and was found to
633 be closely associated with several GGP-type traits, such as ddT122 and
634 lgA120~lgA130. The yield trait is important, and we found that some CS
635 RGB-derived traits, such as U_TEX_SV, E_TEX_SV, TPA_SV and FDNIC_SV, and
636 DS RGB-derived traits, such as M_TEX_TV, U_TEX_TV, E_TEX_TV and GPA_TV,
637 were closely related to yield indicators. These different types of traits could be used as

indicators to reflect the salt stress response. We also constructed a robust prediction model (Fig. S3–S5) that could be used to predict the traditionally measured, dynamic and destructively measured traits associated with the salt stress response via a high-throughput phenotyping platform to facilitate the breeding of salt stress-tolerant *B. napus*.

We used two populations to investigate the genetic architecture of the salt stress tolerance of *B. napus* via GWASs and linkage analysis to identify reliable QTLs or genes associated with the salt stress response. We identified 657,136 significant SNPs (~8.57% of the total) associated with different types of traits (Supporting Information Table S12), which showed that they had specific and similar characteristics, indicating very large differences between the CS RGB-derived, DS RGB-derived, hyperspectrum-derived (GGP) and manually measured traits (Fig. 3a). However, there were a large number of redundant, unstable and possible false-positive sites. For the manually measured traits, we found only 5,531 significant candidate SNPs (~0.07% of the total). However, for only the GGP traits, we detected 283,227 SNPs (~3.69% of the total); thus, this process constitutes an effective way to identify additional main and microeffects of SNPs on the salt stress response (Supporting Information Table S12). In addition, 1,197 significant SNPs (21.64% of the 5,531 significant SNPs associated with the traditional traits) were colocalized between the i-traits and manually measured traits (Supporting Information Table S12). Finally, combining our GWAS and QTL mapping colocalization results (Supporting Information Table S12-S13), we ultimately identified 234 candidate genes associated with the salt stress response. Two novel candidate genes, *BnCKX5* and *BnERF3* (Supporting Information Table S12), were then identified among the many colocalized traits. These two genes were also confirmed by haplotype analyses, sequence variation analyses, RNA sequencing (RNA-seq), genetic transformation and functional verification under salt stress (Fig. 4-5; Fig. S7–S12). Compared with previous studies, high-throughput phenotyping-based GWASs are effective for identifying genes or QTLs that are

associated with the salt stress response and have more main and micro-effects, which could also fill research gaps concerning the salt stress response of *B. napus*.

CONCLUSIONS

High-throughput phenotyping is more flexible and efficient for large germplasm populations over time. Combining high-throughput phenotyping and QTL mapping to analyze the genetics of *Brassica napus* in response to salt stress in this study, we are confident that our study reveals major breakthroughs and includes a novel and reliable method to resolve complex agronomic traits associated with the salt stress response of *B. napus*. We ultimately predicted possible candidate genes through strict selection criteria. Nonetheless, notably, some genes or QTLs could be false positives. In this study, only two genes were identified, which is not enough to reveal the mechanism of *B. napus* salt stress tolerance. In the future, we need to validate more candidate genes associated with the salt stress response. Therefore, the combination of data obtained from multiple views with a high-throughput phenotyping platform, GWASs and linkage analysis is a promising way to provide novel insight into the genetic and molecular mechanisms of *B. napus.* Moreover, this approach could also be extended to other complex crop traits.

ACKNOWLEDGEMENTS

This study was supported by National Key Research and Development Plan of China (2016YFD0101000, 2020YFD1000904-1-3), the National Natural Science Foundation of China (31770397, 31800305), Major science and technology projects in Hubei Province, Cooperative funding between Huazhong Agricultural University and Shenzhen Institute of agricultural genomics (SZYJY2021005, SZYJY2021007), Fundamental Research Funds for the Central Universities (2662020ZKPY017, 2021ZKPY006).

AUTHOR CONTRIBUTIONS

L.G., W.Y. and H.F. designed the research. G.Z., J.Z., Y.P., Z.T., Y.T., H.Z., D.L., X.L., L.L., L.Y., C.J., S.F., J.S., Z.G., G.C. and Q.Y. performed the experiments or analyzed the data. K.L. and S.Y. provided 91 ISLs materials. G.Z., H.F., W.Y. and L.G. analyzed the data and wrote the manuscript.

COMPETING INTERESTS

The authors declare no competing interests.

REFERENCES

Aharoni, A., Dixit, S., Jetter, R., Thoenes, E., van Arkel, G., and Pereira, A. (2004). The SHINE Clade of AP2 Domain Transcription Factors Activates Wax Biosynthesis, Alters Cuticle Properties, and Confers Drought Tolerance when Overexpressed in *Arabidopsis*. *Plant Cell* **16**:2463-2480.

Ai-Sheng, Xiong, Hai-Hua, Jiang, Jing, Zhuang, Ri-He, Peng, Xiao-Fen, and Jin (2012). Expression and Function of a Modified AP2/ERF Transcription Factor from *Brassica napus* Enhances Cold Tolerance in Transgenic *Arabidopsis*. *Molecular Biotechnology* **53**: 198–206.

Al-Tamimi, N., Brien, C., Oakey, H., Berger, B., Saade, S., Ho, Y.S., Schmockel, S.M., Tester, M., and Negrao, S. (2016). Salinity tolerance loci revealed in rice using high-throughput non-invasive phenotyping. *Nature Communications* **7**:13342.

Athar, H., Basra, S., Wahid, A., and Jamil, A. (2009). Inducing salt tolerance in canola (*Brassica napus L.*) by exogenous application of glycinebetaine and proline: Response at the initial growth stages. *Pak. J. Bot* **41**:1311-1319.

Awlia, M., Nigro, A., Fajkus, J., Schmoeckel, S.M., Negrao, S., Santelia, D., Trtilek, M., Tester, M., Julkowska, M.M., and Panzarova, K. (2016). High-Throughput Non-destructive Phenotyping of Traits that Contribute to Salinity Tolerance in *Arabidopsis thaliana*. *Frontiers In Plant Science* **7**:1414.

Bates, L.S., Waldren, R.P., and Teare, I.D. (1973). Rapid Determination of Free Proline for Water-Stress Studies. *Plant and Soil* **39**:205-207.

Berkowitz, F.B.M.H.I.M.G.A., and Masmoudi, K. (2007). Overexpression of wheat Na^+/H^+ antiporter *TNHX1* and H^+-pyrophosphatase *TVP1* improve salt- and drought-stress tolerance in *Arabidopsis thaliana* plants. *Journal of Experimental Botany* **58**:301-308.

Campbell, M.T., Knecht, A.C., Berger, B., Brien, C.J., Wang, D., and Walia, H. (2015). Integrating Image-Based Phenomics and Association Analysis to Dissect the Genetic Architecture of Temporal Salinity Responses in Rice. *Plant Physiology* **168**:1476-1489.

Chen, D., Neumann, K., Friedel, S., Kilian, B., Chen, M., Altmann, T., and Klukas, C. (2014b). Dissecting the Phenotypic Components of Crop Plant Growth and Drought Responses Based on High-Throughput Image Analysis. *Plant Cell* **26**:4636-4655.

Fischer, U., and Droge-Laser, W. (2004). Overexpression of *NtERF5,* a New Member of the Tobacco Ethylene Response Transcription Factor Family Enhances Resistance to Tobacco mosaic virus. *Molecular Plant-Microbe Interactions* **17**:1162-1171.

Gao, S., Zhang, H., Tian, Y., Li, F., Zhang, Z., Lu, X., Chen, X., and Huang, R. (2008). Expression of *TERF1* in rice regulates expression of stress-responsive genes and enhances tolerance to drought and high-salinity. *Plant Cell Reports* **27**:1787-1795.

Gaxiola, R.A., Li, J.L., Undurraga, S., Dang, L.M., and Fink, G.R. (2001). Drought- and salt-tolerant plants result from overexpression of the *AVP1* H^+-pump. *Proceedings of the National Academy of Ences* **98**:11444-11449.

Ge, Y., Bai, G., Stoerger, V., and Schnable, J.C. (2016). Temporal dynamics of maize plant growth, water use, and leaf water content using automated high throughput RGB

and hyperspectral imaging. *Computers and Electronics in Agriculture* **127**:625-632.

Ge, Y., Atefi, A., Zhang, H., Miao, C., Ramamurthy, R.K., Sigmon, B., Yang, J., and Schnable, J.C. (2019). High-throughput analysis of leaf physiological and chemical traits with VIS-NIR-SWIR spectroscopy: a case study with a maize diversity panel. *Plant Methods* **15**:66.

Guo, Z., Yang, W., Chang, Y., Ma, X., Tu, H., Xiong, F., Jiang, N., Feng, H., Huang, C., Yang, P., et al. (2018). Genome-Wide Association Studies of Image Traits Reveal Genetic Architecture of Drought Resistance in Rice. *Mol Plant* **11**:789-805.

He, Y., Wu, D., Wei, D., Fu, Y., Cui, Y., Dong, H., Tan, C., and Qian, W. (2017). GWAS, QTL mapping and gene expression analyses in *Brassica napus* reveal genetic control of branching morphogenesis. *Scientific Reports* **7**:15971.

Hickey, L.T., A, N.H., Robinson, H., Jackson, S.A., Leal-Bertioli, S.C.M., Tester, M., Gao, C., Godwin, I.D., Hayes, B.J., and Wulff, B.B.H. (2019). Breeding crops to feed 10 billion. N*ature Biotechnology* **37**:744-754.

Holland, J., Nyquist, W., and Cervantes-Martínez, C. (2010). *Plant Breeding Reviews*, **22**: 9-112.

Huang, X., Zhao, Y., Wei, X., Li, C., Wang, A., Qiang, Z., Li, W., Guo, Y., Deng, L., and Zhu, C. (2012). Genome-wide association study of flowering time and grain yield traits in a worldwide collection of rice germplasm. *Nature Genetics* **44**:32.

Jian, H.J., Xiao, Y., Jia-Na, L.I., Zhen-Zhen, M.A., and Liu, L.Z. (2014). QTL Mapping for Germination Percentage under Salinity and Drought Stresses in *Brassica napus L. Using a SNP Genetic Map. Acta Agronomica Sinica* **40**:629.

Julkowska, M.M., and Testerink, C. (2015). Tuning plant signaling and growth to survive salt. *Trends in Plant Science* **20**:586-594.

Kang, Y., Torres-Jerez, I., An, Z., Greve, V., Huhman, D., Krom, N., Cui, Y., and Udvardi, M. (2019). Genome-wide association analysis of salinity responsive traits in *Medicago truncatula*. *Plant, cell & environment* **42**:1513-1531.

Karaba, A., Dixit, S., Greco, R., Aharoni, A., Trijatmiko, K.R., Marsch-Martinez, N., Krishnan, A., Nataraja, K.N., Udayakumar, M., and Pereira, A. (2007). Improvement of water use efficiency in rice by expression of *HARDY*, an *Arabidopsis* drought and salt tolerance gene. *Proceedings of the National Academy of Sciences* **104**:15270-15275.

Khedr, and A., H.A. (2003). Proline induces the expression of salt-stress-responsive proteins and may improve the adaptation of Pancratium maritimum L. to salt-stress. *Journal of Experimental Botany* **54**:2553-2562.

Kumar, K., Kumar, M., Kim, S.R., Ryu, H., and Cho, Y.G. (2013). Insights into genomics of salt stress response in rice. *Rice* (N Y) **6**:27.

Lang, L., Xu, A., Ding, J., Zhang, Y., Zhao, N., Tian, Z., Liu, Y., Wang, Y., Liu, X., Liang, F., et al. (2017). Quantitative Trait Locus Mapping of Salt Tolerance and Identification of Salt-Tolerant Genes in *Brassica napus L*. *Frontiers in Plant Science* **8**:1000.

Li, B., Chen, L., Sun, W., Wu, D., Wang, M., Yu, Y., Chen, G., Yang, W., Lin, Z.,

Zhang, X., et al. (2020a). Phenomics-based GWAS analysis reveals the genetic architecture for drought resistance in cotton. *Plant Biotechnology Journal* **18**:2533-2544.

Li, C., Jiang, D., Wollenweber, B., Li, Y., Dai, T., and Cao, W. (2011). Waterlogging pretreatment during vegetative growth improves tolerance to waterlogging after anthesis in wheat. *Plant Science* **180**:672-678.

Li, H., and Durbin, R. (2009). Fast and accurate short read alignment with Burrows-Wheeler transform. *Bioinformatics* 25:1754-1760.

Li, H., Feng, H., Guo, C., Yang, S., Huang, W., Xiong, X., Liu, J., Chen, G., Liu, Q., Xiong, L., et al. (2020b). High-throughput phenotyping accelerates the dissection of the dynamic genetic architecture of plant growth and yield improvement in rapeseed. *Plant Biotechnology Journal* **18**:2345-2353.

Listgarten, J., Lippert, C., and Heckerman, D. (2013). FaST-LMM-Select for addressing confounding from spatial structure and rare variants. *Nature Genetics* **45**:470-471.

Liu, P., Zhang, C., Ma, J.-Q., Zhang, L.-Y., Yang, B., Tang, X.-Y., Huang, L., Zhou, X.-T., Lu, K., and Li, J.-N. (2018). Genome-Wide Identification and Expression Profiling of Cytokinin Oxidase/Dehydrogenase (*CKX*) Genes Reveal Likely Roles in Pod Development and Stress Responses in Oilseed Rape (*Brassica napus L.*). *Genes (Basel)* **9**:168.

Ma, Y.-y., Zheng, L., Xie, R., He, S.-l., and Deng, L. (2016). Genome-wide identification and analysis of *CKX* genes in *Poncirus trifoliata*. *Journal of Horticultural Science and Biotechnology* **91**:592-602.

Meng, L., Li, H., Zhang, L., and Wang, J. (2015). QTL IciMapping: Integrated software for genetic linkage map construction and quantitative trait locus mapping in biparental populations - ScienceDirect. *Crop Journal* **3**:269-283.

Morton, M.J.L., Awlia, M., Al-Tamimi, N., Saade, S., Pailles, Y., Negrao, S., and Tester, M. (2019). Salt stress under the scalpel - dissecting the genetics of salt tolerance. *Plant Journal: for cell and molecular biology* **97**:148-163.

Munns, R., and Tester, M. (2008). Mechanisms of salinity tolerance. *Annual Review of Plant Biology* **59**:651-681.

Qadir, M., and Oster, J.D. (2004). Crop and irrigation management strategies for saline-sodic soils and waters aimed at environmentally sustainable agriculture. *Science of the Total Environment* **323**:1-19.

Savitch, L.V., Allard, G., Seki, M., Robert, L.S., Tinker, N.A., Huner, N., Shinozaki, K., and Singh, J. (2005). The Effect of Overexpression of Two -like Transcription Factors on Photosynthetic Capacity and Freezing Tolerance in *Brassica napus. Plant Cell Physiol* **46**:1525-1539.

Shao, H.B., Liang, Z.S., and Shao, M.A. (2005). Changes of anti-oxidative enzymes and MDA content under soil water deficits among 10 wheat (Triticum aestivum L.) genotypes at maturation stage. *Colloids & Surfaces B Biointerfaces* **45**:7-13.

Shi, H., Quintero, F.J., Pardo, J.M., and Zhu, J.K. (2002). The Putative Plasma Membrane Na^+/H^+ Antiporter *SOS1* Controls Long-Distance Na+ Transport in Plants.

Plant Cell **14**:465-477.

Shi, L., Shi, T., Broadley, M.R., White, P.J., Long, Y., Meng, J., Xu, F., and Hammond, J.P. (2013). High-throughput root phenotyping screens identify genetic loci associated with root architectural traits in *Brassica napus* under contrasting phosphate availabilities. *Ann Bot* **112**:381-389.

Song, C.-P., Agarwal, M., Ohta, M., Guo, Y., Halfter, U., Wang, P., and Zhu, J.-K. (2005). Role of an *Arabidopsis* AP2/EREBP-Type Transcriptional Repressor in Abscisic Acid and Drought Stress Responses. *Plant Cell* **17**:2384-2396.

Song, J.M., Guan, Z., Hu, J., Guo, C., Yang, Z., Wang, S., Liu, D., Wang, B., Lu, S., Zhou, R., et al. (2020). Eight high-quality genomes reveal pan-genome architecture and ecotype differentiation of *Brassica napus*. *Nature Plants* **6**:34-45.

Song, W., and Liu, M. (2017). Farmland Conversion Decreases Regional and National Land Quality in China. *Land Degradation & Development* **28**:459-471.

Tang, S., Zhao, H., Lu, S., Yu, L., Zhang, G., Zhang, Y., Yang, Q.Y., Zhou, Y., Wang, X., Ma, W., et al. (2021). Genome- and transcriptome-wide association studies provide insights into the genetic basis of natural variation of seed oil content in *Brassica napus*. *Mol Plant* **14**:470-487.

Tester, M., and Davenport, R. (2003). Na^+ tolerance and Na^+ transport in higher plants. *Ann Bot* **91**:503-527.

Tyerman, S.D., and Munns, R. (2019). Energy Costs of Salinity Tolerance In Crop Plants. **221**:25-29.

Wan, H., Chen, L., Guo, J., Li, Q., Wen, J., Yi, B., Ma, C., Tu, J., Fu, T., and Shen, J. (2017). Genome-Wide Association Study Reveals the Genetic Architecture Underlying Salt Tolerance-Related Traits in Rapeseed (*Brassica napus L.*). *Frontiers In Plant Science* **8**:593.

Wang, Y.X., Sun, G.R., Wang, J.B., Cao, W.Z., and Lu, Z.H. (2006). Relationships among MDA content, plasma membrane permeability and the chlorophyll fluorescence parameters of *Puccinellia tenuiflora* seedlings under NaCl stress. *Acta Ecologica Sinica* **26**:122-129.

Wani, A.S., Ahmad, A., Hayat, S., and Fariduddin, Q. (2013). Salt-induced modulation in growth, photosynthesis and antioxidant system in two varieties of *Brassica juncea. Saudi Journal of Biological Sciences* **20**:183-193.

Wu, D., Liang, Z., Yan, T., Xu, Y., Xuan, L., Tang, J., Zhou, G., Lohwasser, U., Hua, S., Wang, H., et al. (2019). Whole-Genome Resequencing of a Worldwide Collection of Rapeseed Accessions Reveals the Genetic Basis of Ecotype Divergence. *Mol Plant* **12**:30-43.

Wu, X., Feng, H., Wu, D., Yan, S., Zhang, P., Wang, W., Zhang, J., Ye, J., Dai, G., Fan, Y., et al. (2021). Using high-throughput multiple optical phenotyping to decipher the genetic architecture of maize drought tolerance. *Genome Biology* **22**:185.

Xiaqing, Wang, Ruyang, Zhang, Wei, Song, Liang, Han, Xiaolei, and Liu (2019). Dynamic plant height QTL revealed in maize through remote sensing phenotyping using a high-throughput unmanned aerial vehicle (UAV). *Scientific Reports* **9**:3458.

Yamaguchi, T., and Blumwald, E. (2005). Developing salt-tolerant crop plants: challenges and opportunities. *Trends In Plant Science* **10**:615-620.

Yang, W., Feng, H., Zhang, X., Zhang, J., Doonan, J.H., Batchelor, W.D., Xiong, L., and Yan, J. (2020). Crop Phenomics and High-Throughput Phenotyping: Past Decades, Current Challenges, and Future Perspectives. *Mol Plant* **13**:187-214.

Yang, W., Guo, Z., Huang, C., Duan, L., Chen, G., Jiang, N., Fang, W., Feng, H., Xie, W., Lian, X., et al. (2014). Combining high-throughput phenotyping and genome-wide association studies to reveal natural genetic variation in rice. *Nature Communications* **5**:5087.

Zhang, B., Liu, C., Wang, Y., Yao, X., Wang, F., Wu, J., King, G.J., and Liu, K. (2015). Disruption of a CAROTENOID CLEAVAGE DIOXYGENASE 4 gene converts flower colour from white to yellow in *Brassica* species. *New Phytologist* **206**:1513-1526.

Zhang, H.-X., Hodson, J.N., Williams, J.P., and Blumwald, E. (2001). Engineering salt-tolerant *Brassica* plants: Characterization of yield and seed oil quality in transgenic plants with increased vacuolar sodium accumulation. *Proceedings of the National Academy of Sciences* **98**:12832.

Zhang, Z., and Huang, R. (2010). Enhanced tolerance to freezing in tobacco and tomato overexpressing transcription factor TERF2/LeERF2 is modulated by ethylene biosynthesis. *Plant Molecular Biology* **73**:241-249.

Zhou, X., and Stephens, M. (2012). Genome-wide efficient mixed-model analysis for association studies. *Nature Genetics* **44**:821-824.

Zhu, J.-K. (2001). The salinity challenge. *New Phytologist* **225**:1047-1048.

FIGURE LEGENDS

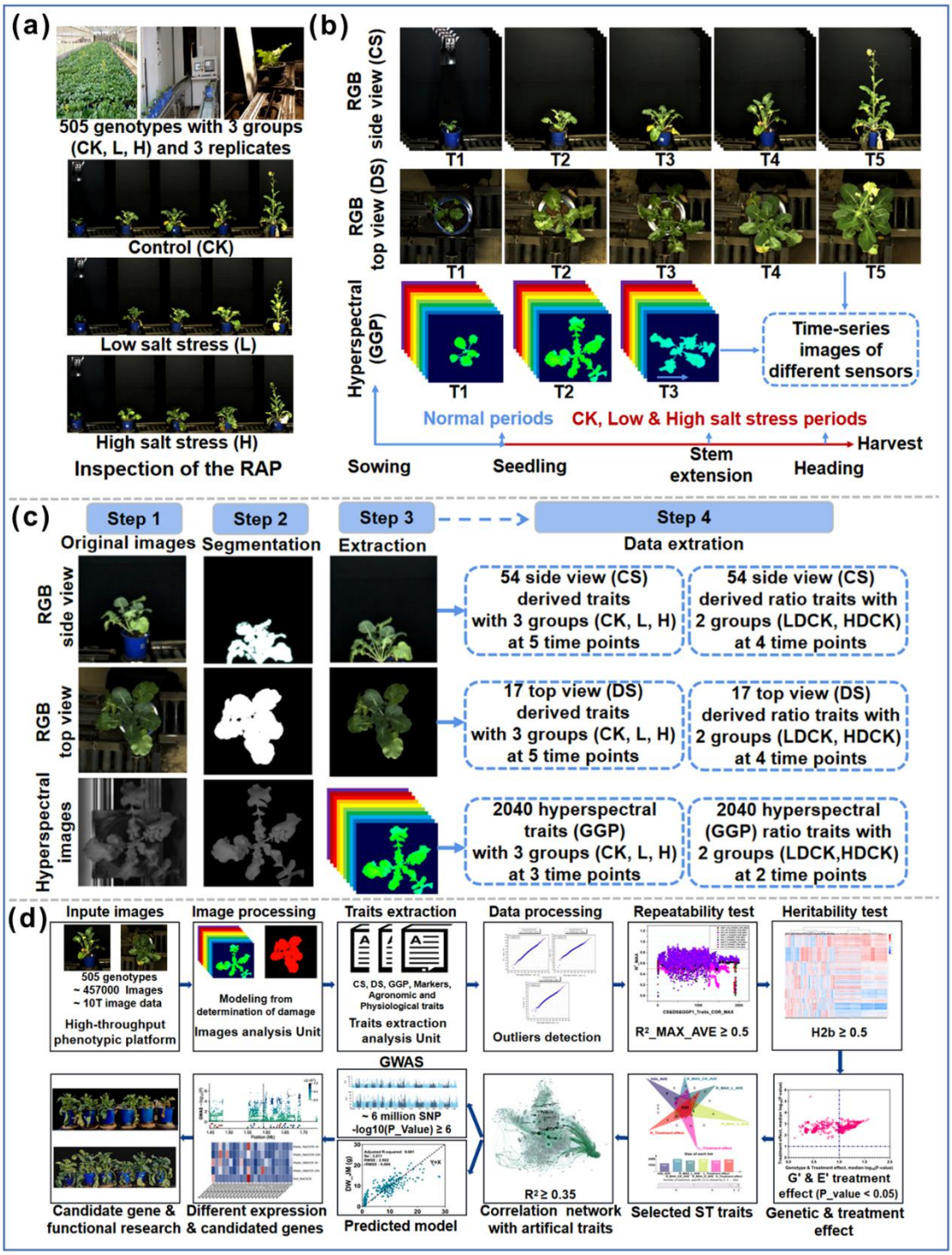

Fig. 1 Experimental design and data analysis pipeline.

(a) High-throughput phenotyping platform and experimental design.

(b) CS and DS RGB-derived and GGP images and trait measurements via a high-throughput phenotyping platform over time under low and high salt stress conditions.

(c) High-throughput phenotyping image analysis and trait extraction (see Materials and Methods).

(d) Flow chart of the data analysis (see Materials and Methods).

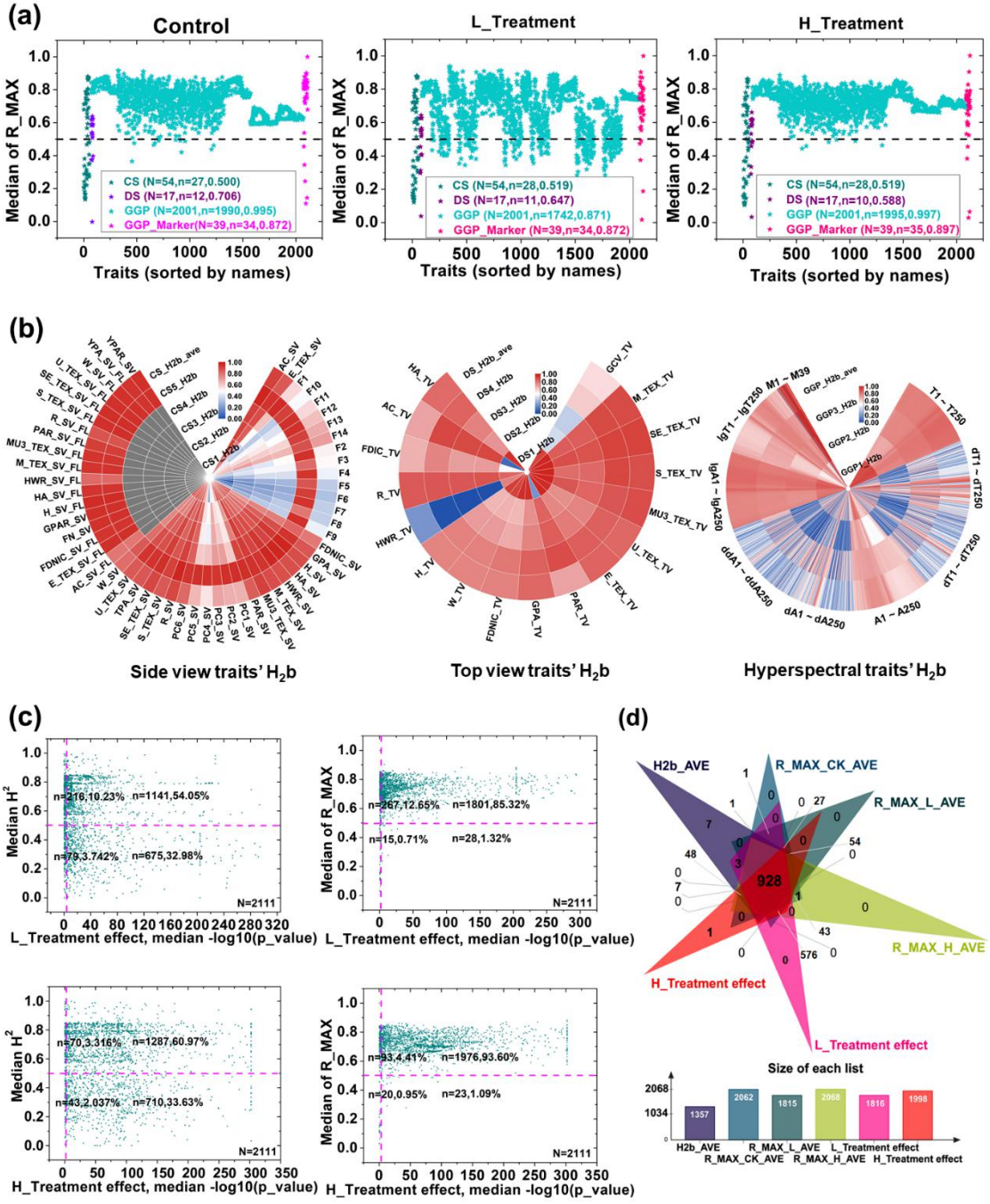

Fig. 2 Determination of effective traits with high repeatability, high heritability and significant treatment effects.

(a) Repeatability refers to the maximum correlation coefficient of 3 replicates under control (R_MAX_CK), low salt (R_MAX_L) and high salt (R_MAX_H) stress conditions.

(b) H2b of CS RGB-derived traits (CS' H2b), DS RGB-derived traits (DS' H2b) and hyperspectrum-derived traits (GGP' H2b) over time.

928 **(c)** Assessment of the repeatability (median of R_MAX), heritability (median of H2b)
929 and low salt and high salt treatment effects of i-traits via a scatter plot (L_treatment
930 effect, H_treatment effect, median negative log-transformed p-values).
931 **(d)** Reliable i-traits related to the salt stress response with high reproducibility, high
932 heritability and a significant treatment effect were determined, as shown by a Venn
933 diagram.
934
935

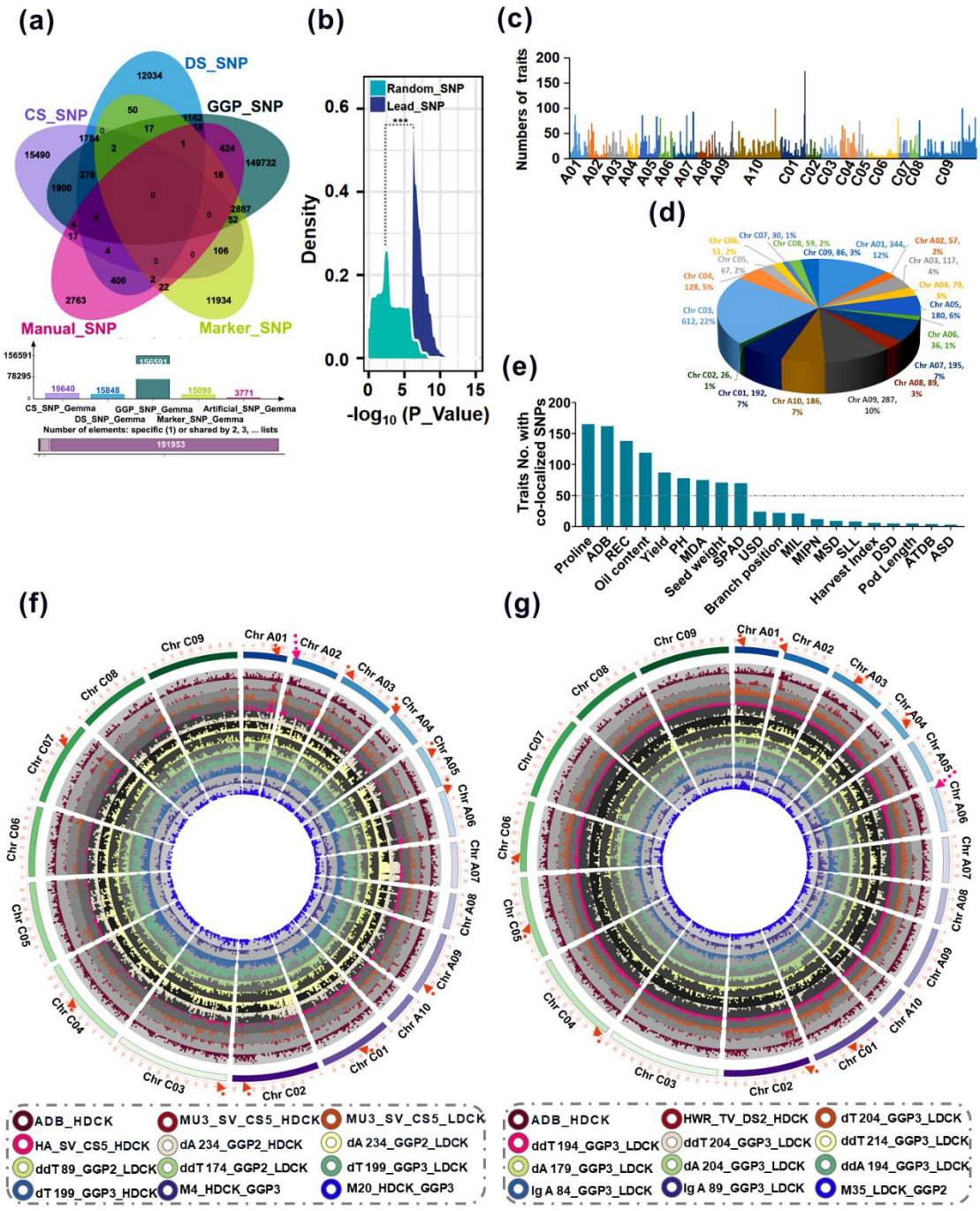

Fig. 3 GWASs and candidate genes.

(a) Candidate SNPs associated with different types of traits (CS, DS, GGP and manually measured traits), as shown by a Venn diagram.

(b) Density plot showing the P-value distribution of significant SNPs of the candidate and randomly selected SNPs. Permutation tests with randomly selected SNPs were compared to those of the candidate SNPs. Statistical significance was determined via Student's t-test: *, $P < 0.05$; **, $P < 0.01$; ***, $P < 0.001$.

(c) Number of traits with colocalized SNPs on chromosomes.

(d) Number of traits with high frequencies of colocalized SNPs (≥ 10) on chromosomes.

(e) Number of traits with colocalized SNPs between manually measured traits and i-traits.

(f-g) Circular Manhattan plots of multiple traits (P-value ≤ 1E–4) with colocalized SNPs on ChrA02 (f) and ChrA06 (g).

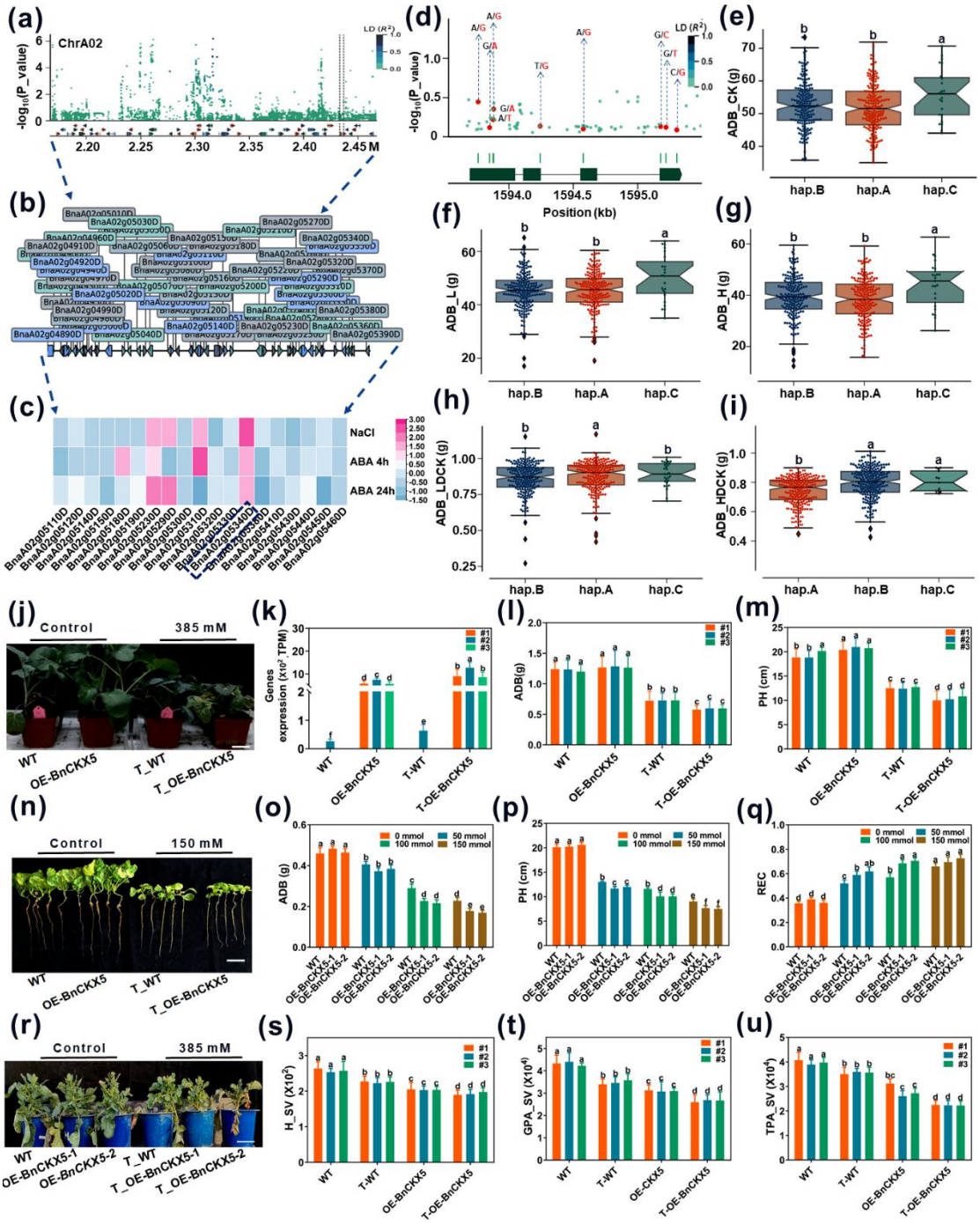

953

954 **Fig. 4 Determination of the function of the *BnCKX5* gene in plants under salt**
955 **stress.**

956 **(a)** Part of the Manhattan plots of loci colocalized on ChrA02. The points represent
957 the log-transformed P-values of variants identified via a GWAS of STC of ABD
958 (ADB_HDCK). The bottom of the Manhattan plots shows several candidate genes on
959 ChrA02.

960 **(b)** Candidate genes within 200 kb upstream or downstream of significant SNPs.

(c) Differential expression of candidate genes within 200 kb upstream or downstream of significant SNPs of plants under ABA (25 μM solution conditions; 4 h and 24 h) and salt stress (385 mM NaCl; one week).

(d) SNP variants of *BnCKX5* labeled with red points on ChrA02.

(e-i) Boxplots of haplotypes for absolute and relative ADB values of different stress conditions and controls via high-throughput phenotyping based on the haplotypes of *BnCKX5* among the 505 accessions (ADB_CK, e; ADB_L, f; ADB_H, g; ADB_LDCK, h; ADB_HDCK, i). The values are the means ± SDs (n = 3 replicates), and the different letters indicate differences at $P \leq 0.05$ according to two-way ANOVA.

(j-m) Comparison of the gene expression (k), ADW (l) and PH (m) of Westar WT and *OE-BnCKX5* plants under control and salt stress conditions (0 mM, 385 mM NaCl; two weeks; J). Bars = 5 cm. The values are the means ± SDs (n = 6 replicates), and the different letters indicate differences at $P \leq 0.05$ according to two-way ANOVA.

(n-q) Comparison of the ADW (o), PH (p) and REC (q) of Westar WT and *OE-BnCKX5* plants under control and salt stress conditions (0 mM, 50 mM, 100 mM and 150 mM NaCl, two weeks; n; Fig. S8a–c). Bars = 10 cm. The values are the means ± SDs (n = 8 replicates), and the different letters indicate differences at $P \leq 0.05$ according to two-way ANOVA.

(r-u) Comparison of H_SV (s), GPA_SV (t) and TPA_SV (u) of Westar WT plants and *OE-BnCKX5* plants via the high-throughput phenotyping platform (0 mM and 385 mM NaCl; two weeks; r). Bars = 10 cm. Additional traits are shown in Fig. S9a–b. The values are the means ± SDs (n = 8 replicates), and the different letters indicate differences at $P \leq 0.05$ according to two-way ANOVA.

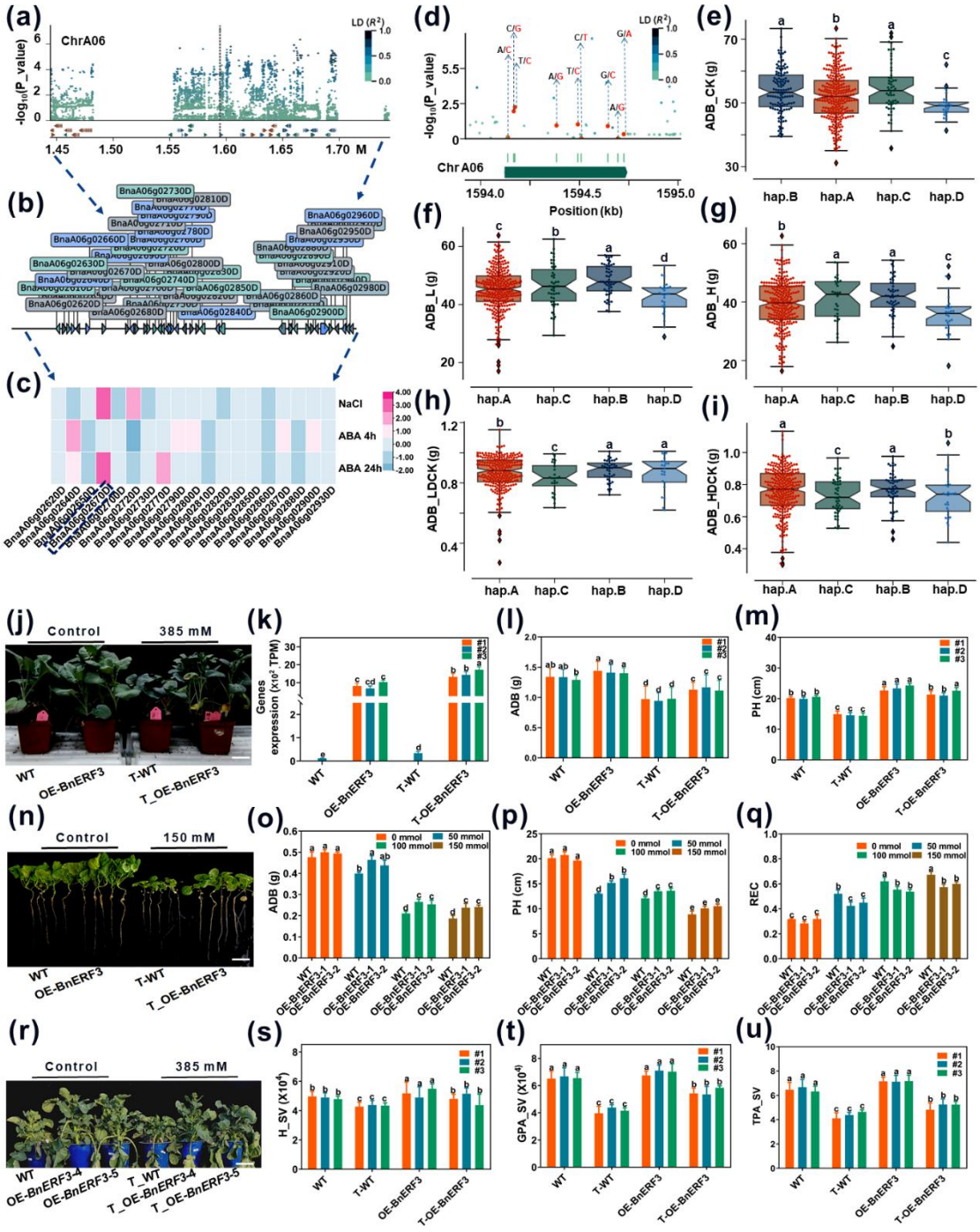

Fig. 5 Determination of the function of the *BnERF3* gene under salt stress.

(a) Part of the Manhattan plots of loci colocalized on ChrA06. The points represent the log-transformed P-values of variants via a GWAS of STC of ADW (ADB_HDCK). The bottom of the Manhattan plots shows several candidate genes on ChrA06.

(b) Candidate genes within 200 kb upstream or downstream of significant SNPs.

(c) Differential expression of candidate genes within 200 kb upstream or downstream of significant SNPs in plants under ABA (25 μM solution conditions; 4 h and 24 h) and salt stress (385 mM NaCl; one week).

(d) SNP variants of *BnERF3* labeled with red points on ChrA06.

(e-i) Boxplots of haplotypes for absolute and relative ADB values under different stress conditions and control conditions according to high-throughput phenotyping based on the haplotypes of *BnERF3* among the 505 accessions (ADB_CK, e; ADB_L, f; ADB_H, g; ADB_LDCK, h; ADB_HDCK, i). The values are the means ± SDs (n = 3 replicates), and the different letters indicate differences at $P \leq 0.05$ according to two-way ANOVA.

(j-m) Comparison of the gene expression (k), ADW (l) and PH (m) of Westar WT and *OE-BnERF3* plants under control and salt stress conditions (0 mM and 385 mM NaCl; two weeks, j). Bars = 5 cm. The values are the means ± SDs (n = 6 replicates), and the different letters indicate differences at $P \leq 0.05$ according to two-way ANOVA.

(n-q) Comparison of the ADW (o), PH (p) and REC (q) of Westar WT and *OE-BnERF3* plants under control and salt stress conditions (0 mM, 50 mM, 100 mM and 150 mM NaCl; two weeks; n; Fig. S11a–c). Bars = 10 cm. The values are the means ± SDs (n = 8 replicates), and the different letters indicate differences at $P \leq 0.05$ according to two-way ANOVA.

(r-u) Comparison of H_SV (S), GPA_SV (T) and TPA_SV (U) of Westar WT plants and *OE-BnERF3* plants via a high-throughput phenotyping platform (0 mM and 385 mM NaCl; two weeks, R). Bars = 10 cm. Additional traits are shown in Fig. S12a–b. The values are the means ± SDs (n = 8 replicates), and the different letters indicate differences at $P \leq 0.05$ according to two-way ANOVA.

SUPPORTING INFORMATION

Additional Supporting Information may be found online in the Supporting Information section at the end of the article.

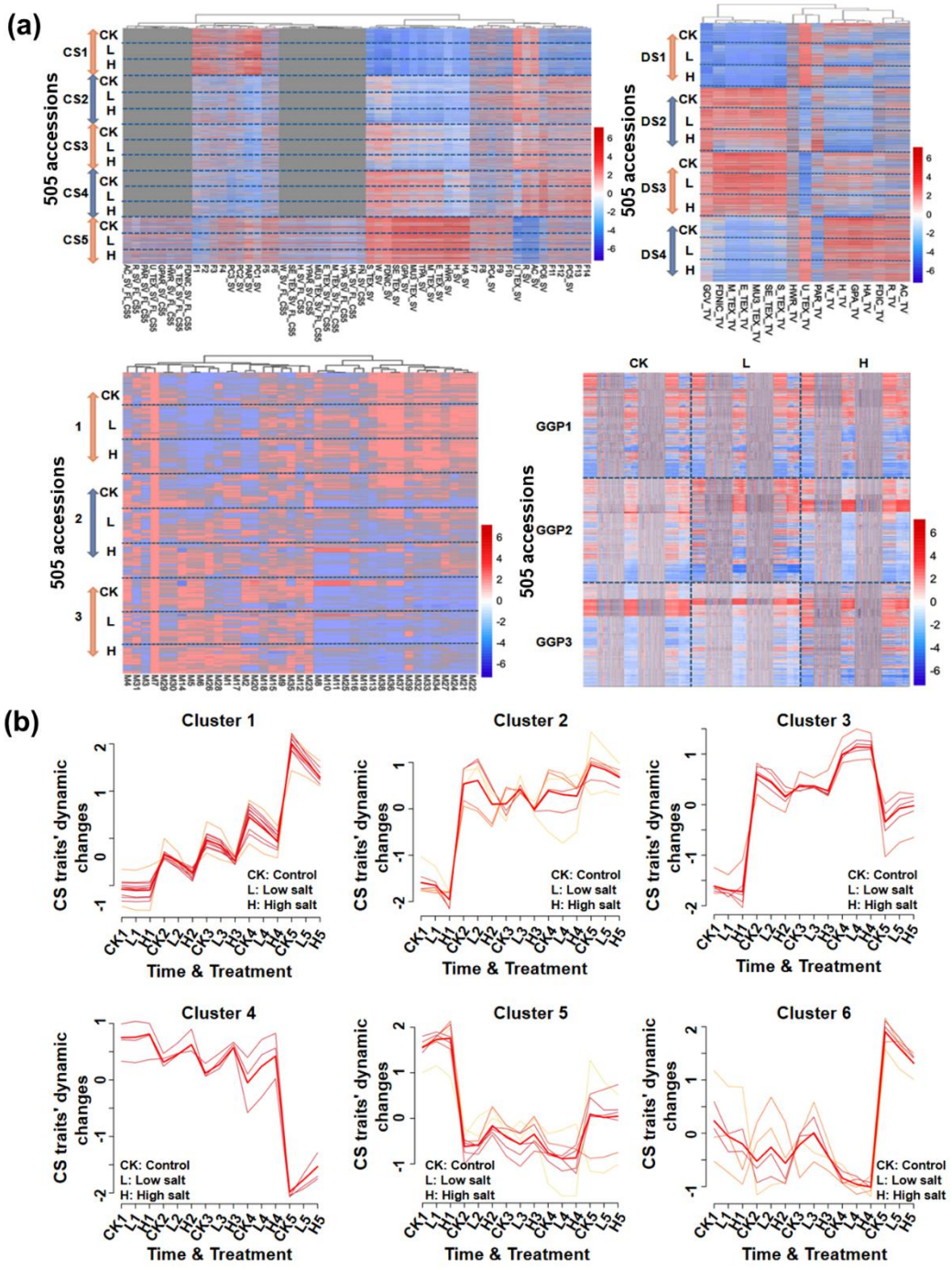

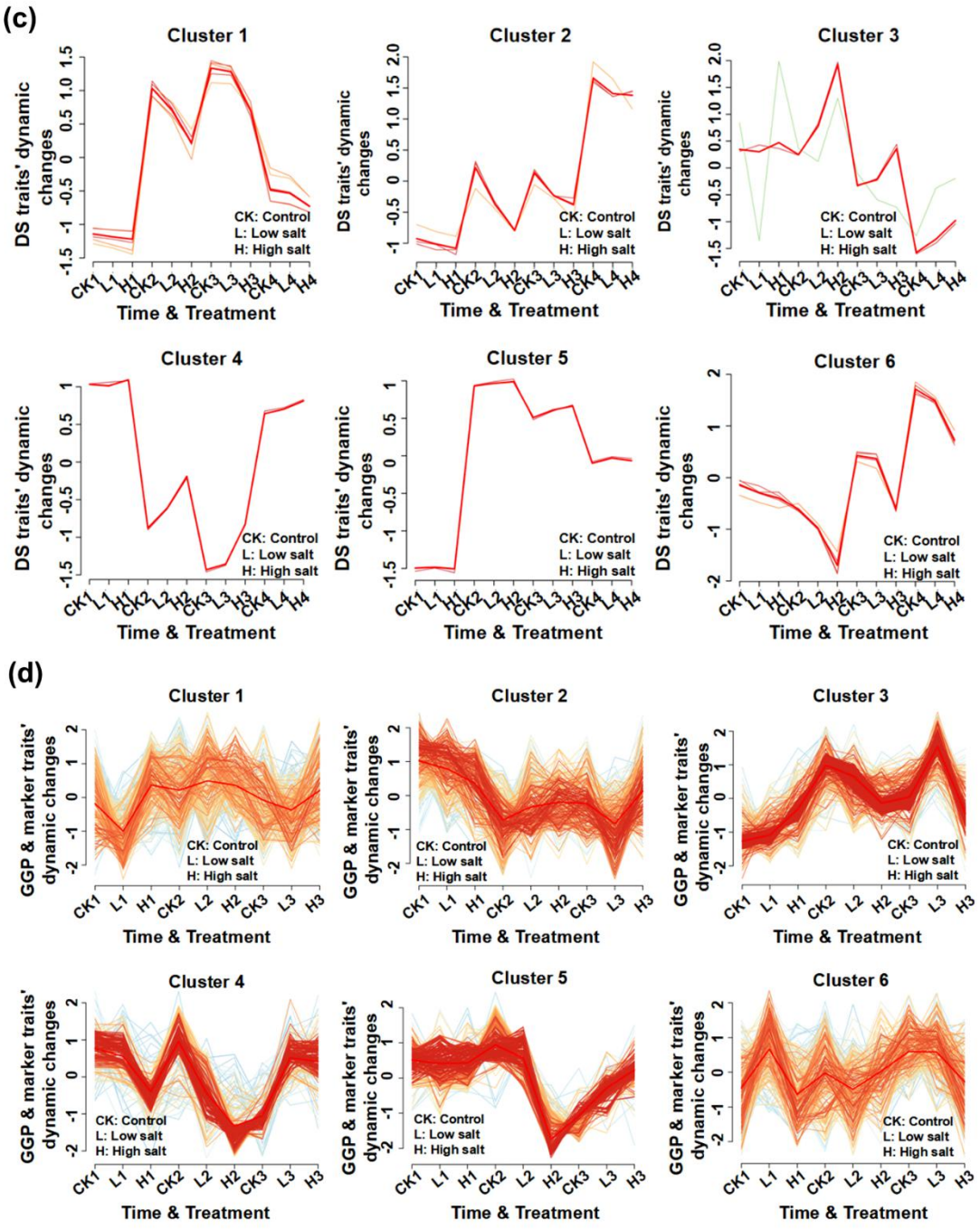

Fig. S1 Dynamic heatmap and cluster diagram for salt stress conditions over time.

(a)

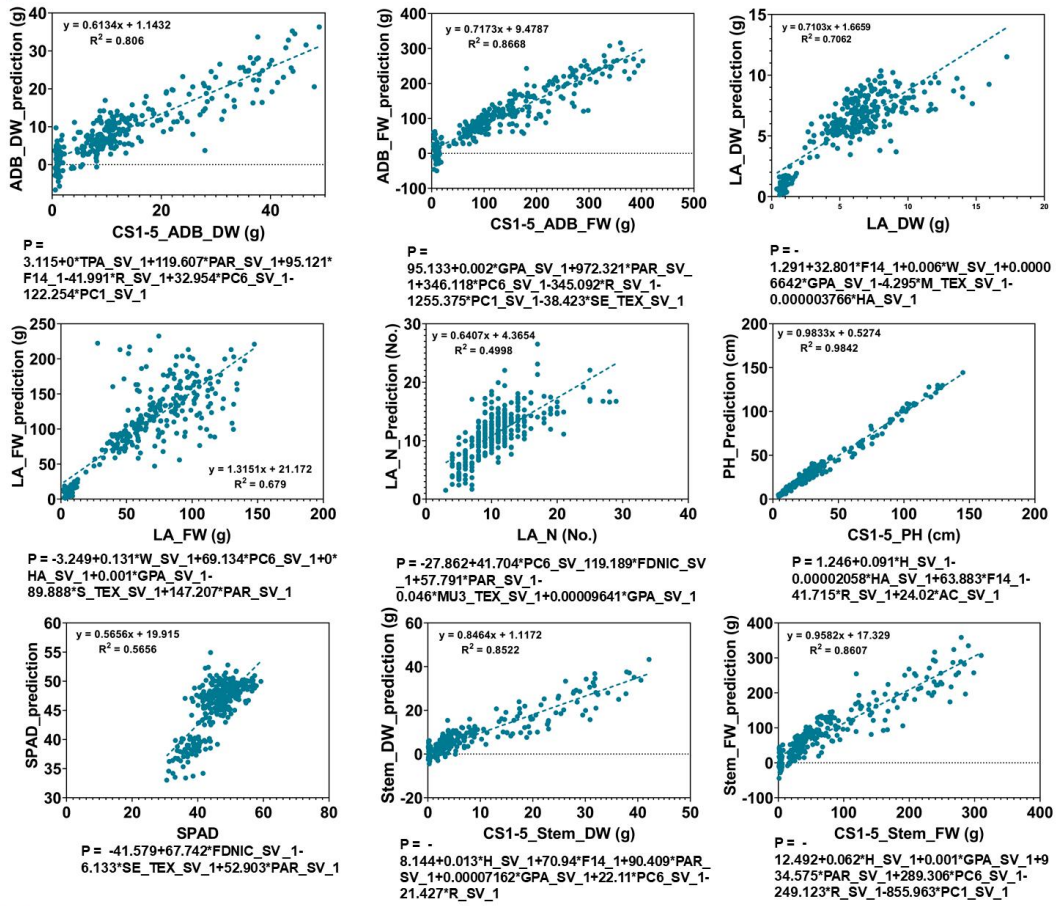

(b)

T1-T5 period of CS prediction parameters

Dependent variable	R2	Independent variables	Sample No.	Independent variables No.
PH_AVE	0.984	H_SV, HA_SV, F14, R_SV, AC_SV	300	5
LA_N	0.456	PC6_SV, FDNIC_SV , PAR_SV, MU3_TEX_SV, GPA_SV	300	5
LA_FW	0.822	W_SV, PC6_SV,HA_SV, GPA_SV,S_TEX_SV, PAR_SV	300	6
LA_DW	0.654	F14, W_SV,GPA_SV, M_TEX_SV, HA_SV	300	5
Stem_FW	0.863	H_SV, GPA_SV, PAR_SV, PC6_SV, R_SV, PC1_SV	300	6
Stem_DW	0.852	H_SV, F14, PAR_SV, GPA_SV, PC6_SV, R_SV	300	6
ADB_FW	0.87	GPA_SV, PAR_SV, PC6_SV, R_SV, PC1_SV, SE_TEX_SV	300	6
ADB_DW	0.806	TPA_SV, PAR_SV, F14, R_SV, PC6_SV, PC1_SV	300	6
SPAD	0.566	FDNIC_SV , SE_TEX_SV, PAR_SV	300	3

Fig. S2 Prediction model for manually measured traits of plants under salt stress conditions from CS RGB-derived traits at T1–T5.

(a)

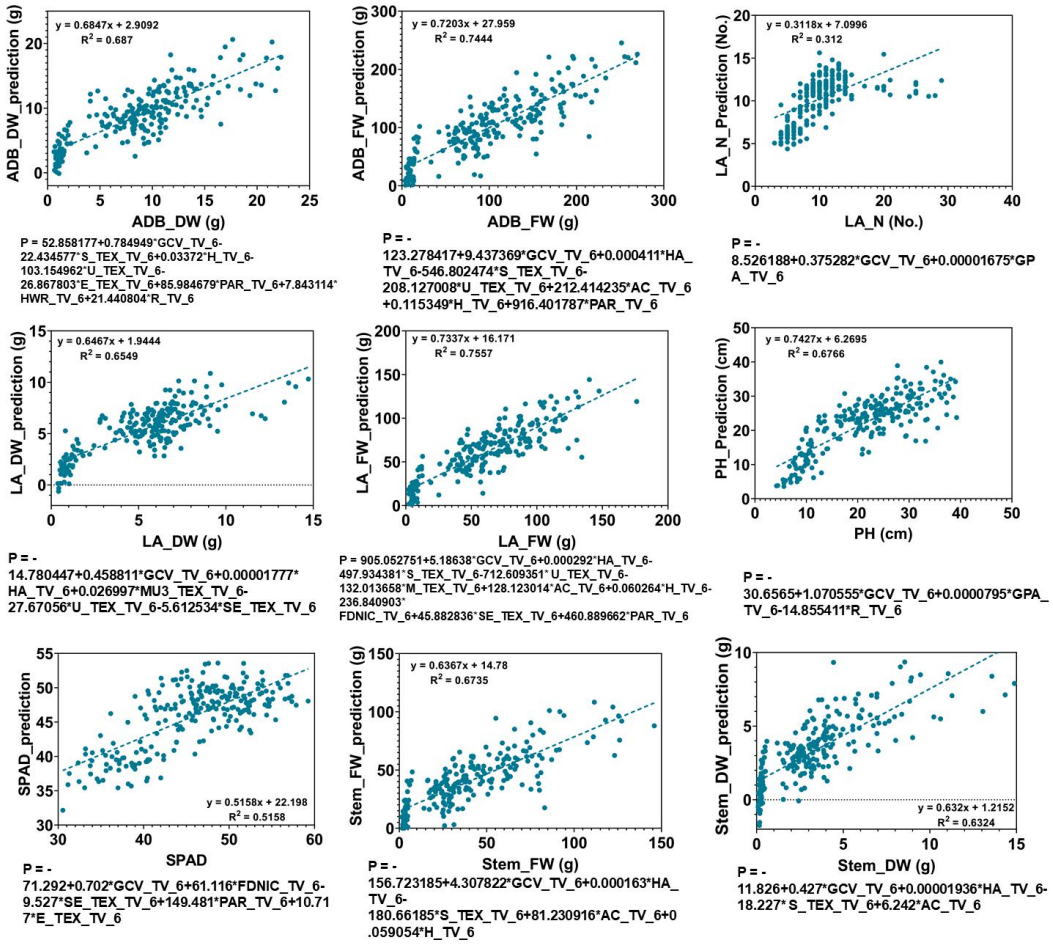

(b)

T1-T4 period of DS prediction parameters

Dependent variable	R2	Independent variables	Sample No.	Independent variables No.
PH	0.677	GCV_TV, GPA_TV, R_TV	240	3
LA_N	0.312	GCV_TV, GPA_TV	240	2
LA_FW	0.756	GCV_TV, HA_TV, S_TEX_TV, U_TEX_TV, M_TEX_TV, AC_TV, H_TV, FDNIC_TV, SE_TEX_TV, PAR_TV	240	10
LA_DW	0.655	GCV_TV, HA_TV, MU3_TEX_TV, U_TEX_TV, SE_TEX_TV	240	5
Stem_FW	0.685	GCV_TV, HA_TV, S_TEX_TV, AC_TV, H_TV	240	5
Stem_DW	0.632	GCV_TV, HA_TV, S_TEX_TV, AC_TV	240	4
ADB_FW	0.6735	GCV_TV, HA_TV, S_TEX_TV, U_TEX_TV, AC_TV, H_TV, PAR_TV	240	7
ADB_DW	0.687	GCV_TV, S_TEX_TV, H_TV, U_TEX_TV, E_TEX_TV, PAR_TV, HWR_TV, R_TV	240	8
SPAD	0.516	GCV_TV, FDNIC_TV, SE_TEX_TV, PAR_TV, E_TEX_TV	240	5

Fig. S3 Prediction model for manually measured traits under salt stress conditions from DS RGB-derived traits at T1–T4.

(a)

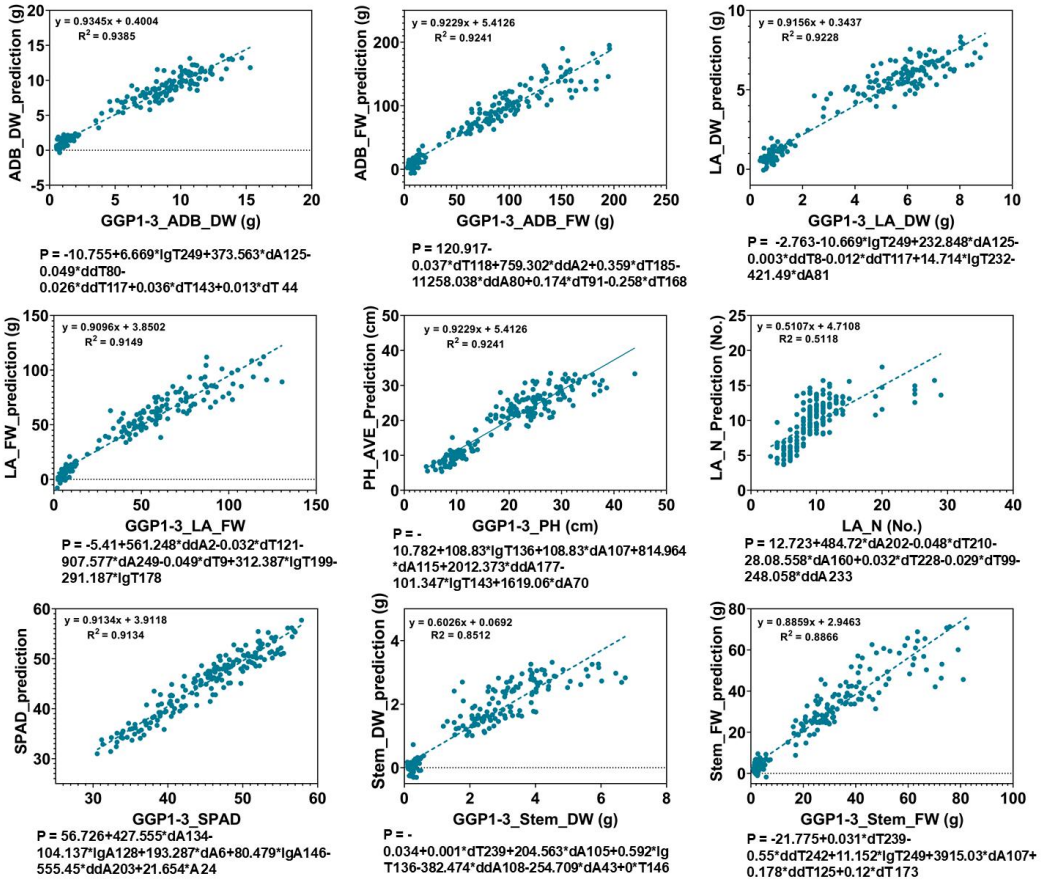

(b)

T1-T3 period of GGP prediction parameters

Dependent variable	R2	Independent variables	Sample No.	Independent variables No.
PH_AVE	0.859	lg T 136, dA 107, dA 115, ddA 177, lg T 143, dA 70	180	6
LA_N	0.512	dA 202, dT 210, dA 160, dT 228, dT 99, ddA 233	180	6
LA_FW	0.915	ddA 2, dT 121, dA 249, dT 9, lg T 199, lg T 178	180	6
LA_DW	0.923	lg T 249, dA 125, ddT 8, ddT 117, lg T 232, dA 81	180	6
Stem_FW	0.887	dT 239, ddT 242, lg T 249, dA 107, ddT 125, dT 173	180	6
Stem_DW	0.881	dT 239, dA 105, lg T 136, ddA 108, dA 43, T 146	180	6
ADB_FW	0.924	dT 118, ddA 2, dT 185, ddA 80, dT 91, dT 168	180	6
ADB_DW	0.938	lg T 249, dA 125, ddT 80, ddT 117, dT 143, dT 44	180	6
SPAD	0.913	dA 134, lg A 128, dA 6, lg A 146, ddA 203, A 24	180	6

Fig. S4 Prediction model for manually measured traits under salt stress conditions based on GGP traits at T1–T3.

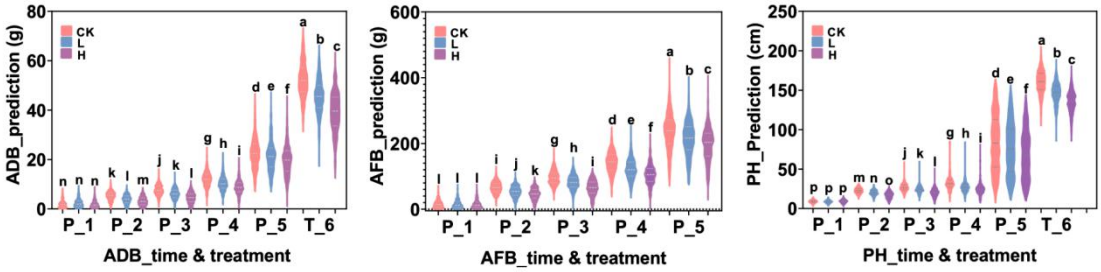

1041

1042 **Fig. S5** Boxplot of ADB, AFB and PH at T1–T6 according to the prediction model.

1043

1044

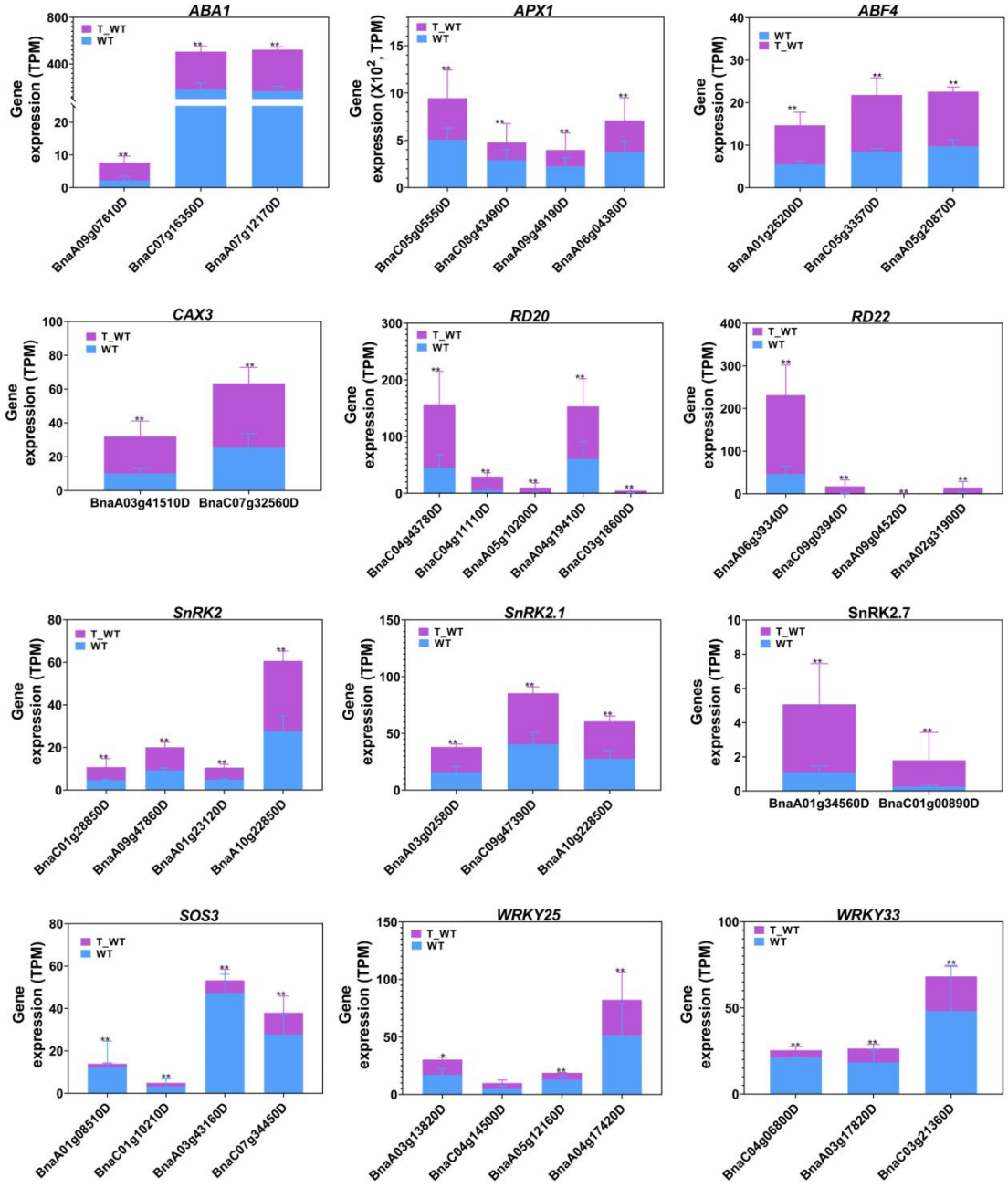

Fig. S6 Expression of genes reportedly associated with salt stress via GWASs.

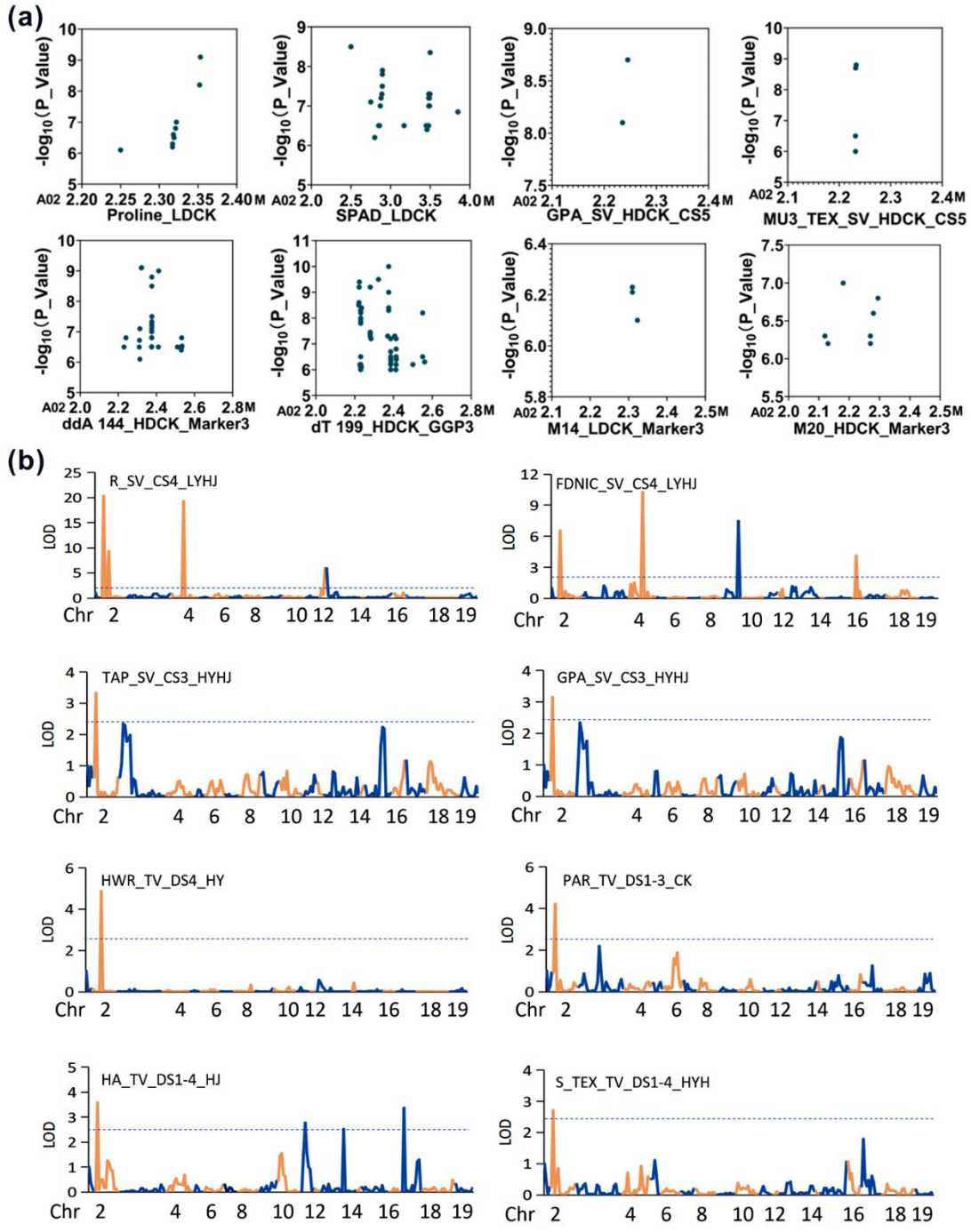

Fig. S7 Colocalization of loci identified on ChrA02 according to GWASs and linkage analysis.

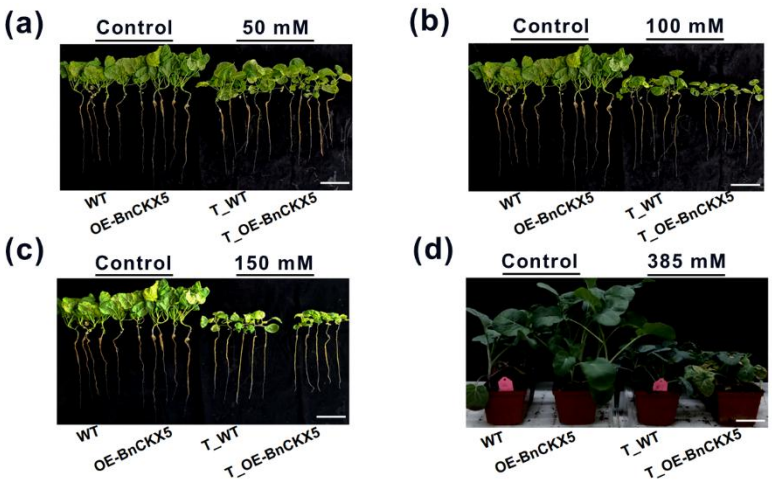

Fig. S8 Westar WT and *OE-BnCKX5* plants grown in solution and in soil.

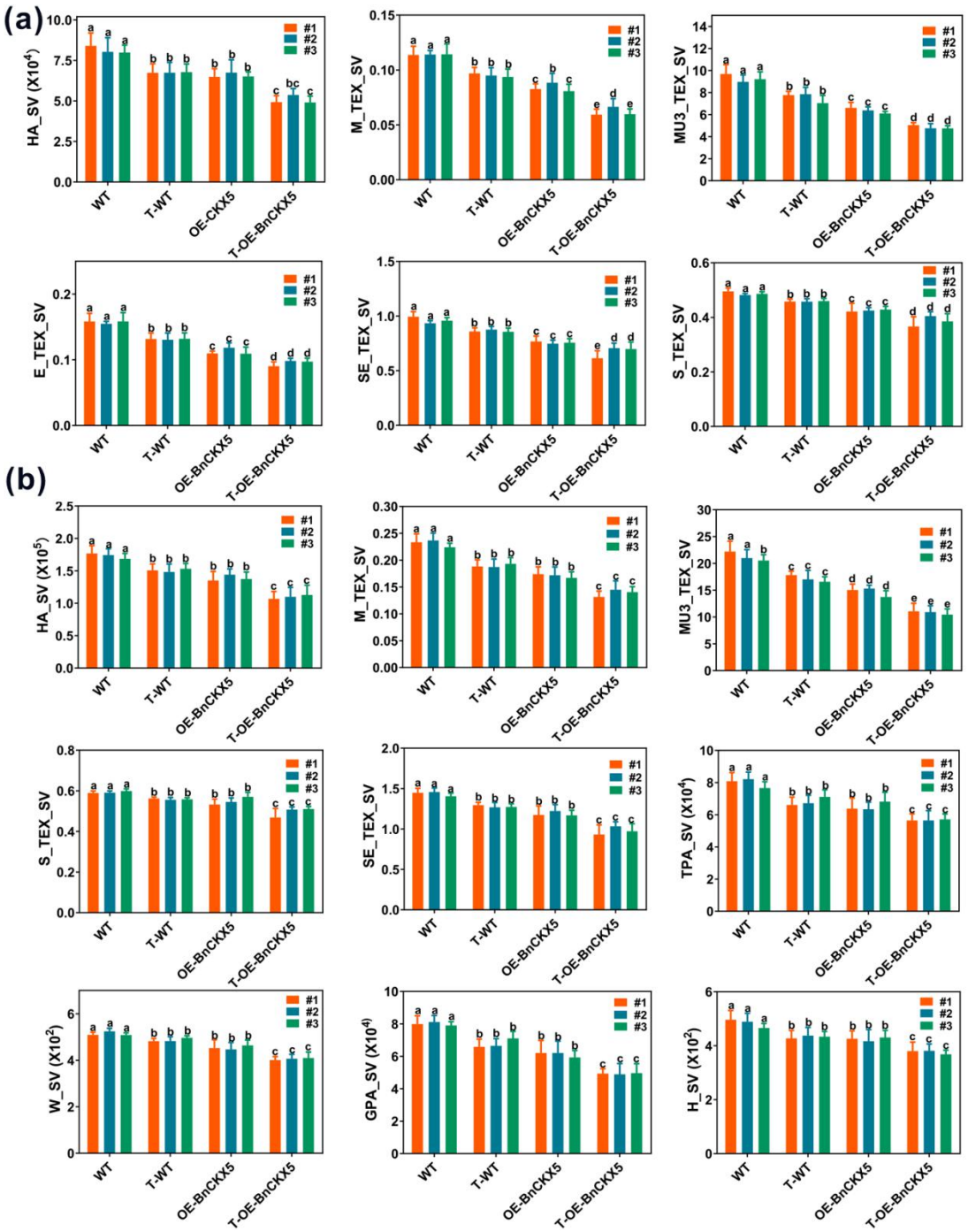

Fig. S9 Westar WT and *OE-BnCKX5* plants on the high-throughput phenotyping platform.

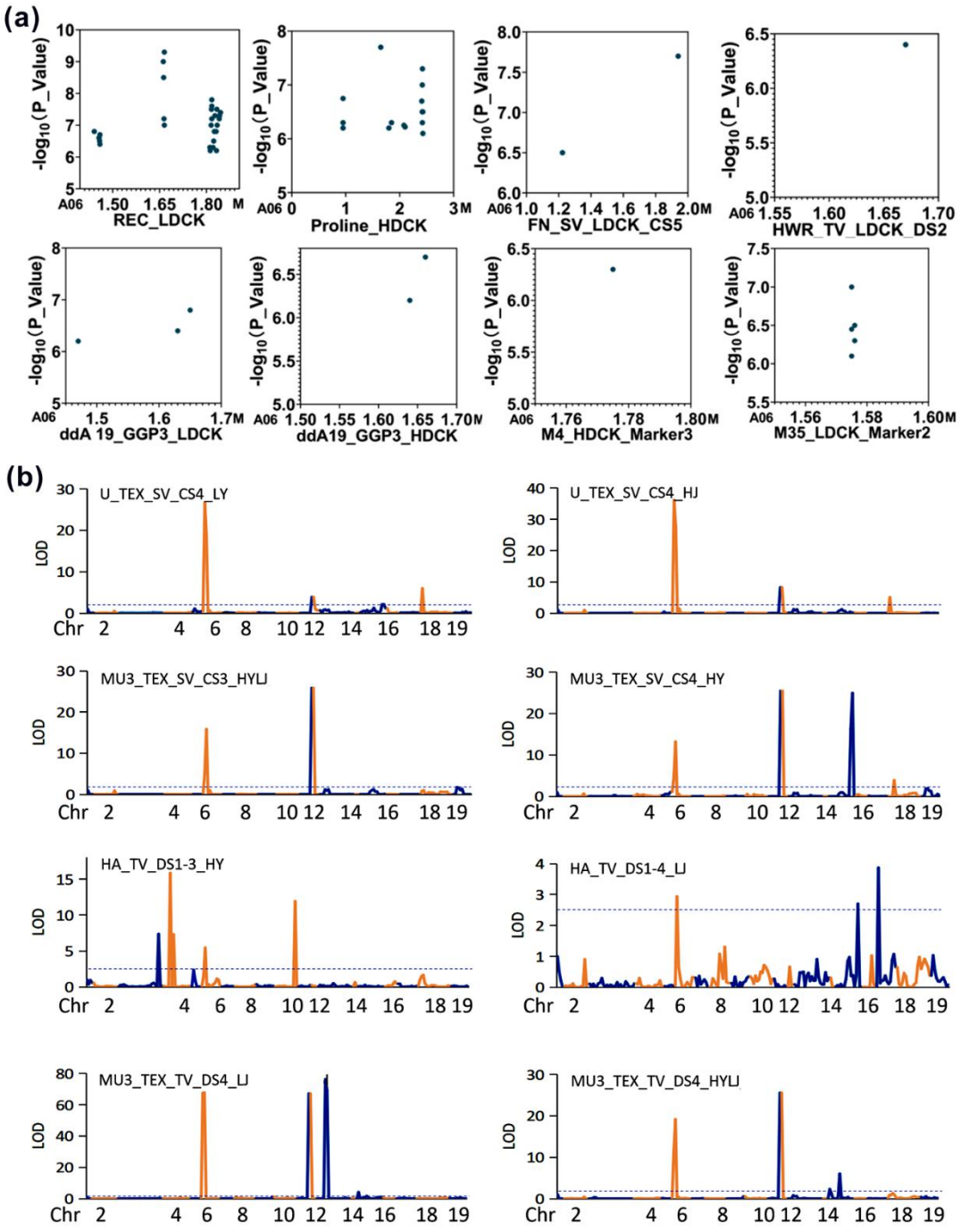

Fig. S10 Colocalization of loci on ChrA06 identified via GWASs and linkage analysis.

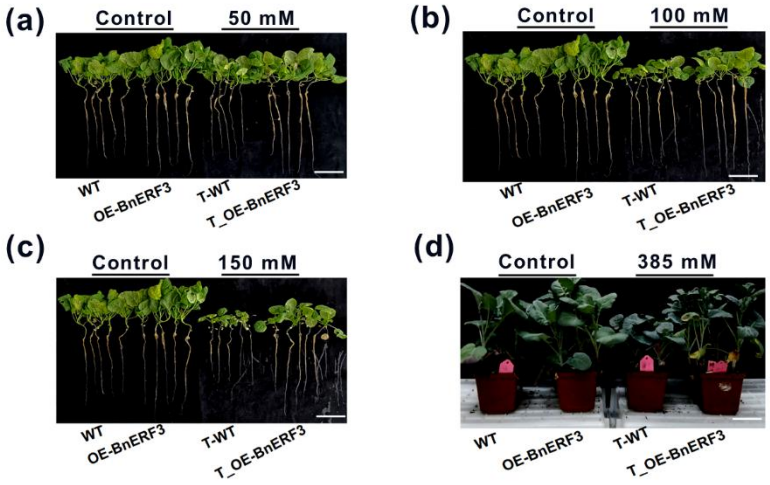

Fig. S11 Westar WT and *OE-BnERF3* plants grown in solution and in soil.

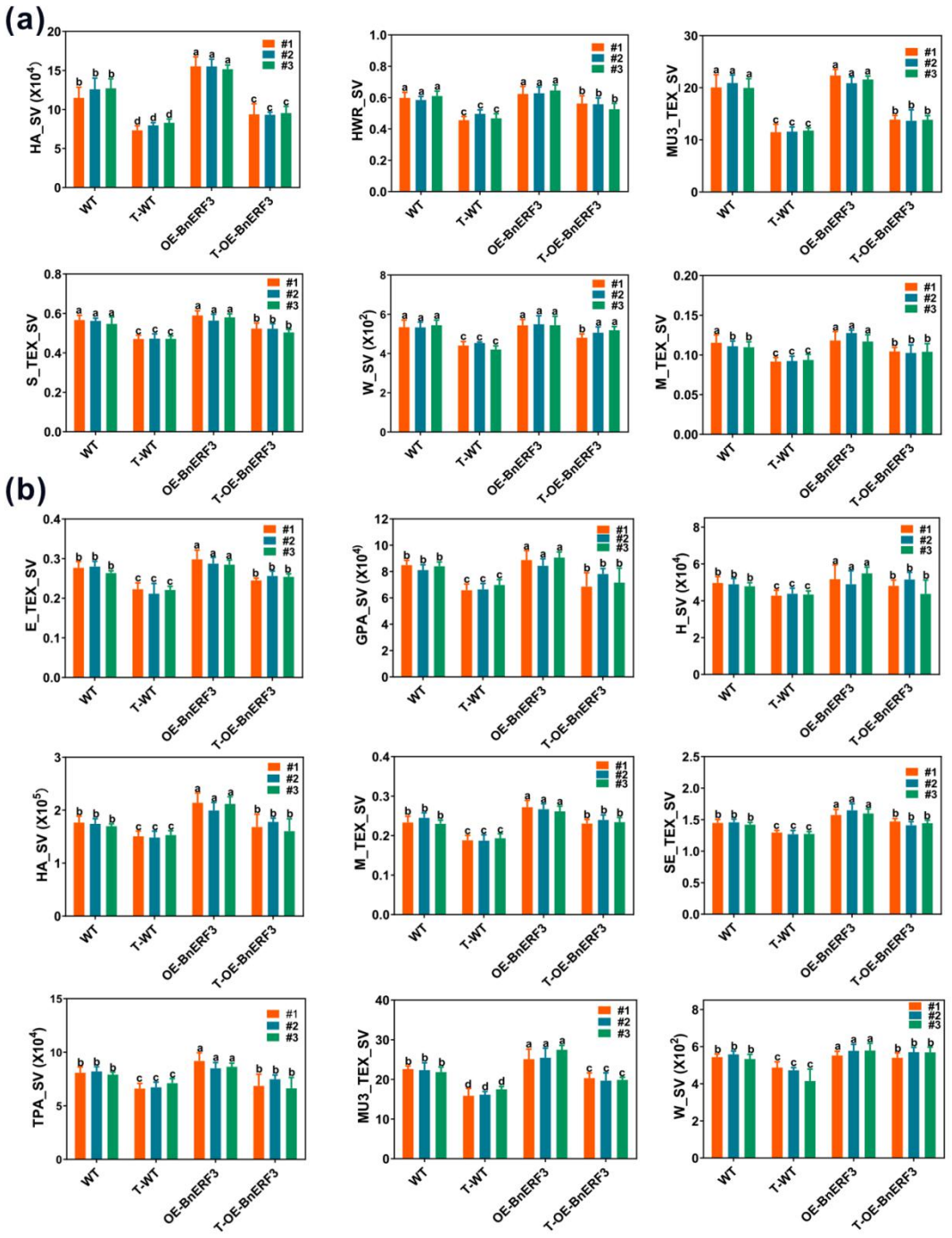

Fig. S12 Westar WT and *OE-BnERF3* plants on the high-throughput phenotyping platform.

SUPPLEMENTAL TABLES

Table S1 Description of the 505 *B. napus* accessions and 91 ISLs.

Table S2 Treatment conditions and data collection dates for the 505 *B. napus* accessions and 91 ISLs.

Table S3 Description of all the measured traits.

Table S4 CS RGB-derived traits of the 505 *B. napus* accessions and 91 ISLs.

Table S5 DS RGB-derived traits of the 505 *B. napus* accessions and 91 ISLs.

Table S6. Hyperspectral (GGP) traits of the 505 accessions.

Table S7 Destructive Sampling.

Table S8 Descriptive statistics of the 505 *B. napus* accessions and 91 ISLs.

Table S9 High-quality traits with a significant L&H_treatment effect, high H_2B and a high R_MAX' were identified via Venn diagrams.

Table S10 Prediction models and 5-fold cross validation.

Table S11 Data for GWASs and linkage analysis.

Table S12 Candidate SNPs and genes identified via GWASs.

Table S13 Candidate loci identified via linkage analysis.

Table S14 Sequence variation and haplotypes analyses of *BnCKX5* and *BnERF3*.

Table S15 RNA-seq of the *OE-BnCKX5*, *OE-BnERF3* and WT plants.

Table S16 Primers used in this study.

Table S17 Data collection dates and weather conditions.